

# WINGS: a Wide-field Nearby Galaxy-cluster Survey. I: Optical imaging

G. Fasano<sup>1</sup>, C. Marmo<sup>2,3</sup>, J. Varela<sup>1</sup>, M. D'Onofrio<sup>4</sup>, B. M. Poggianti<sup>1</sup>, M. Moresco<sup>5</sup>,  
E. Pignatelli<sup>1</sup>, D. Bettoni<sup>1</sup>, P. Kjærgaard<sup>6</sup>, L. Rizzi<sup>7</sup>, W. Couch<sup>8</sup>, and A. Dressler<sup>9</sup>

<sup>1</sup> INAF - Padova Astronomical Observatory, Vicolo Osservatorio 5, 35122 Padova, Italy

<sup>2</sup> CEA/DAPNIA, Service d'Astrophysique, Gif-sur-Yvette, France

<sup>3</sup> Institut d'Astrophysique de Paris, 98 bis bd Arago, 75014 Paris, France

<sup>4</sup> Astronomy Department, University of Padova, Vicolo Osservatorio 2, 35122 Padova, Italy

<sup>5</sup> Instituto de Astrofísica de Andalucía (CSIC) Apartado 3004, 18080 Granada, Spain

<sup>6</sup> Copenhagen University Observatory. The Niels Bohr Institute for Astronomy Physics and Geophysics, Juliane Maries Vej 30, 2100 Copenhagen, Denmark

<sup>7</sup> Institute for Astronomy, University of Hawaii, 2680 Woodlawn Drive, Honolulu, HI 96822, USA

<sup>8</sup> School of Physics, University of New South Wales, Sydney 2052, Australia

<sup>9</sup> Observatories of the Carnegie Institution of Washington, Pasadena, CA 91101, USA

Received <date> / Accepted <date>

**Abstract.** This is the first paper of a series that will present data and scientific results from the WINGS project, a wide-field, multiwavelength imaging and spectroscopic survey of galaxies in 77 nearby clusters. The sample was extracted from the ROSAT catalogs of X-ray emitting clusters with constraints on the redshift ( $0.04 < z < 0.07$ ) and distance from the galactic plane ( $|b| < 20$  deg).

The global goal of the WINGS project is the systematic study of the local cosmological variance of the cluster population and of the cluster galaxies as a function of cluster properties and local environment. This data collection will allow to define a local, Zero-Point reference to gauge the cosmological evolution when compared to more distant clusters.

The core of the project consists of wide-field optical imaging of the selected clusters in the B and V bands. We have also completed a multi-fiber, medium-resolution spectroscopic survey for 51 of the clusters in the master sample. The imaging and spectroscopy data were collected using respectively the WFC3 INT and WYFFOS@WHT in the northern hemisphere, and the WFI@MPG and 2dF@AAT in the southern one. In addition, a NIR (J, K) survey of 50 clusters and an H<sub>α</sub> survey of some 10 clusters have been also programmed.

In this paper we briefly outline the global objectives and the main characteristics of the WINGS project. Moreover, the observing strategy and the data reduction of the optical imaging survey (WINGS-OPT) are presented. We have achieved a photometric accuracy of 0.02 mag, reaching completeness to V = 23.5. Field size and resolution (FWHM) span the absolute intervals (1.6-2.7) Mpc and (0.7-1.7) kpc, respectively, depending on the redshift and on the seeing. This allows the planned studies to get a valuable description of the local properties of clusters and galaxies in clusters.

**Key words.** Galaxies - Clusters of galaxies - Photometry

## 1. Introduction

Galaxies of different morphology are not evenly distributed. Hubble & Humason (1931) noticed early on that (in the local universe) spiral galaxies are abundant in the field while S0 and elliptical galaxies dominate in denser regions. Gravitational interaction apparently affects the global properties of the galaxies even in low density environments, and even such field galaxies show significant

ifferences with respect to truly isolated systems that have been free of interaction for a long period of time (Varela et al. 2004).

Clusters of galaxies are dense peaks in the galaxy distribution and therefore appropriate sites to look for changes in the properties of the galaxies. They can be therefore used to trace the evolution of the systems themselves as well as that of the galaxies in them. Such a systematic analysis certainly needs a fair knowledge of the properties of local clusters of galaxies and their content (the end point of the evolution), extensive enough to cope

Send offprint requests to: Giovanni Fasano,  
e-mail: fasano@pd.astro.it

not only with the average properties but also with their physical variance. This is unfortunately still lacking. As a matter of fact, while a large amount of high quality data for distant clusters is continuously being gathered from both HST observations and large ground-based telescopes, our present knowledge of the systematic properties of galaxies in nearby clusters, remains surprisingly limited, with Virgo, Coma and Fornax as the main references.

In the  $0.4 \leq z \leq 0.5$  range, exploiting the high spatial resolution achieved with the Hubble Space Telescope (HST), Dressler et al. (1997) and Smail et al. (1997) found that spirals are a factor of 2–3 more abundant and S0 galaxies are proportionally less abundant than in nearby clusters, while the fraction of ellipticals is already as large or larger. This implies significant morphological transformations occurring rather recently. Similarly, using excellent-seeing, ground based imaging with the NOT telescope (La Palma), Fasano et al. (2000) have completed the picture in the range  $0.1 \leq z \leq 0.25$ , showing that the S0 population smoothly grows from  $z = 0.5$  to  $z = 0$ , at the expense of the population of spiral galaxies. They have also highlighted the role that the cluster type plays in determining the relative occurrence of S0 and elliptical galaxies at a given redshift: clusters at  $z = 0.1 - 0.2$  have a low (high) S0/E ratio if they display (lack) a strong concentration of elliptical galaxies towards the cluster centre. This dichotomy seems to support Oemler's (1974) suggestion that elliptical-rich and S0-rich clusters are not two evolutionary stages in cluster evolution, but intrinsically different types of clusters in which the abundance of ellipticals was established at redshifts much greater than 0.5.

That trend is supported by the morphological studies at  $z > 0.5$ , that find an even lower fraction of early-type galaxies (E + S0s), thus indicating that this fraction keeps decreasing up to  $z = 1$  (van Dokkum et al. 2000; Lubin et al. 2002; Simard et al. 2005). The most recent works, based on the Advanced Camera for Surveys, demonstrate that it is the decreasing proportion of S0 galaxies that drives this decline also at  $z = 0.8 - 1$  (Postman et al. 2005; Desai et al. 2005). This change of the morphological mix in clusters is expressed in the evolution of the morphology-density relation with  $z$  (Dressler et al. 1997; Smith et al. 2004; Postman et al. 2005).

The work on intermediate-redshift clusters observed by HST has been complemented with ground-based spectroscopic surveys that have led to a detailed comparison of the spectral and morphological properties (Dressler et al. 1999; Poggianti et al. 1999; Couch et al. 1994, 1998, 2001; Fisher et al. 1998; Lubin et al. 1998; Balogh et al. 1997, 2000). These studies have shown that the spiral population includes most of the star-forming galaxies, a large number of post-starburst galaxies and a sizeable fraction of the red, passive galaxies; in contrast, the stellar populations of (the few) S0 galaxies appear to be as old and passively evolving as those in the ellipticals. These observations are consistent with the post-starburst and star-forming galaxies being recently infallen old spirals whose

star formation is truncated upon entering the cluster and that will evolve into S0's at a later time.

At variance with intermediate-redshift clusters, for which recent, high-quality photometric data are available, the morphological reference for local clusters is still the historical database by Dressler (1980), based on photographic plates, giving the positions, the estimated magnitudes (down to  $V = 16$ ) and the visual morphological classification for galaxies in 55 clusters in the range  $0.011 \leq z \leq 0.066$ . This awkward situation can be easily understood since only with the new large format (wide-field) CCD mosaics cameras a significant number of low redshift clusters could be reasonably well mapped.

Our goal has been to help fill this information gap. Accordingly, we began in 1999 a program to secure a large database for a local sample of clusters, to study the cosmic variance of the cluster properties and their populations in a systematic way. The result would be a reference Zero-Point for comparison with studies at higher  $z$  and for evolutionary studies. To that end we have collected wide-field photometric and spectroscopic data for an X-ray selected sample of 77 clusters at low redshift, spanning a wide range in X-ray and optical properties. The observational requirements have been set to ensure an adequate data quality, both for imaging and spectroscopy, in order to obtain detailed and reliable morphological classifications and estimates of stellar population ages, metallicities and star formation histories.

Similar projects were, in the meantime, also begun, either for smaller samples (e.g. Pimbblet et al. 2001; Christlein & Zabludo 2003), or with more limited goals (Smith et al. 2004). On the spectroscopic side, the ESO Nearby Abell Cluster Survey (ENACS, Katgert et al. 1996; Biviano et al. 1997) collected redshifts for galaxies in 107 clusters, of which 67 with at least 20 spectroscopic members. This dataset yielded information on cluster velocity dispersions, kinematics and spatial distributions of different types of galaxies, that motivated detailed analysis of cluster properties (e.g. Katgert et al. 1998; Biviano et al. 1997, 1999; Mazure et al. 1996). Samples of low-redshift clusters have been also identified based on the redshifts obtained by two recent large spectroscopic surveys, 2dF and Sloan (e.g. de Propris et al. 2003, see Nichol 2004 and Vogeley et al. 2004 for references on Sloan cluster catalogs), the former having no imaging CCD corresponding database. Results based on these surveys have highlighted the strong correlation between star formation properties in galaxies and local galaxy density, and that such correlation exists both inside and outside of clusters (Lewis et al. 2002; Gombez et al. 2003; Kauffmann et al. 2004; Balogh et al. 2004). Unfortunately, given the typical spatial resolution of the imaging and the magnitude limit of the SDSS, it is not immediate to make a detailed comparison with the existing high redshift morphological and spectroscopic studies.

This paper is the first of a series presenting the results of this project, that we have called WINGS for Wide-Field Nearby Galaxy-Cluster Survey. The goal of the present

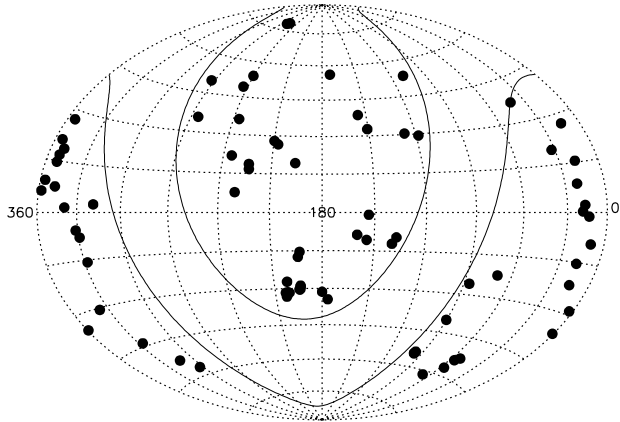


Fig. 1. A full-sky map of the cluster sample (equatorial coordinates). Lines delimiting the region  $|b| < 20$  are drawn.

paper is to outline the objectives and the main characteristics of the W INGS program (Sec. 2) and to describe in detail the optical imaging observations. The selection of the cluster sample is presented in Sec. 3, while Sec. 4 and 5 are devoted to the description of the observations and the procedures for the reduction of the optical wide-field data, respectively. The data quality of optical imaging is analysed in Sec. 8. Finally, a brief summary of the future plans concerning the whole W INGS project is given in Sec. 9.

In this and in the following papers of the series we assume the now standard metric with  $H_0 = 70$ ,  $m = 0.3$  and  $\Omega = 0.7$ .

## 2. The W INGS project

The principal goal of the W INGS project is to elaborate a statistically meaningful, high quality database of the properties of nearby clusters of galaxies and of the galaxies that populate them. Hopefully, this will contribute to improve our knowledge of clusters and cluster galaxies in the local universe and will provide the reference to gauge the changes with redshift over their physical variance at a given  $z$ .

In broad terms, the goals of the project are to characterize the global properties of clusters taken as systems, and those of their member galaxies. Among the former ones, we include their total luminosity and size, the velocity dispersion, the presence of substructures and the cluster scaling relations (Mardi et al. 2004), apart the already existing data on the X-ray luminosity. This will permit to explore the existence of well-defined relations between structural parameters and characterize the actual range of those properties.

Regarding the member galaxies, our primary goals are to analyze the variance of the morphological fractions

(E/S0/S/Irr), their distribution in the clusters and the morphology-density relation. The analysis of the colors and the spectral information will provide the data necessary to retrace the star formation history of galaxies in nearby clusters.

The W INGS project was designed to cover all these topics. Originally it was planned as a wide-field optical ( $B, V$ ) imaging survey of an X-ray selected sample of nearby clusters of galaxies. This is the core of the project, called W INGS-OPT from now on. The strategy for imaging and for the resulting data reduction are the main subject of the present article.

Besides, other surveys were designed and carried out to complement the characterization of the cluster galaxies. The already completed W INGS-SPE survey consists of multi-fiber spectroscopy of galaxies in 51 clusters from the master W INGS sample, obtained with the WYFFOS@WHT and the 2dF@AAT spectrographs over the same area covered by the optical imaging ( $34^{\circ} \times 34^{\circ}$ ). The spectra cover the range 3800–7000 Å (WYFFOS) and 3600–8000 Å (2dF), with dispersions of 3 Å and 9 Å, respectively, for the galaxies with  $V < 20$  (between 100 and 300 per cluster). This limit is 1.5 and 2.0 mag deeper than the 2dF and Sloan surveys, respectively.

Two more follow-up surveys of clusters in the W INGS sample are presently ongoing. The first one is a NIR (W INGS-NIR: J and K bands) imaging survey, with the new Wide-Field Camera at the UKIRT telescope. This will obtain data for 50 clusters, useful at providing an estimate of the stellar mass of galaxies, as well as constraining the spectral energy distribution of galaxies in these fields. The other one is an H survey (W INGS-HAL), with the WFC@INT camera and purpose-designed narrow-band filters, to image 1 square degree of 10 W INGS clusters. Finally, a very-wide-field (1 square degree) optical survey (W INGS-VWF), with the ESO-VST telescope, equipped with OmegaCam, has been programmed for the near future.

Altogether these data will constitute a multiwavelength photometric and spectroscopic dataset which will allow detailed studies of the properties of nearby clusters of galaxies, and cope with their variance, necessary to identify the cosmic evolution when compared with those of higher redshift systems.

We present here the observations, data reduction and analysis of data quality from W INGS-OPT. We have obtained information about astrometry, integrated and surface photometry and morphology for galaxies in our fields. For all galaxies down to the limit of detectability we have extracted the position, size, concentration, average attenuating and orientation, as well as the integrated and aperture photometry in the two observed bands,  $B, V$ . For a subsample of large galaxies we have also obtained detailed surface photometry (luminosity and geometrical profiles) and global structural parameters (total magnitudes, effective radii, ellipticity and Sérsic index) using our tool for automatic surface photometry (GASP-HOT, Pignatelli et al. 2005). Finally, morphological type estimates of the same

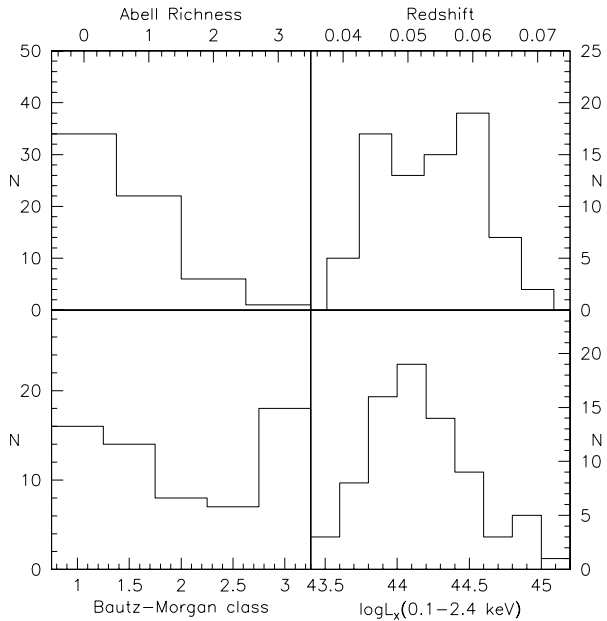


Fig. 2. Distribution of some cluster properties in the W INGS sample

subsample of large galaxies, compared and calibrated with visual classifications, were automatically obtained with a purposely-written tool M ORPHOT: Fasano et al. in preparation).

The Catalogues and the analysis of the different properties will be presented in subsequent papers of this series. To maximize the scientific outcome of the data, the whole W INGS dataset and products, including photometric, surface photometry, morphological and spectroscopic catalogs, will become publicly available as the corresponding papers of this series are published.

### 3. The cluster sample

To investigate in a systematic way the correlations between cluster properties and cluster galaxy populations, a well-defined, large cluster sample is required, with available X-ray data and covering a wide range in optical and X-ray properties.

W INGS clusters have been selected from three X-ray flux limited samples compiled from ROSAT All-Sky Survey data: the ROSAT Brightest Cluster Sample (BCS, Ebeling et al. 1998), and its extension (eBCS, Ebeling et al. 2000) in the Northern hemisphere and the X-Ray-Brightest Abell-type Cluster sample (XBACS, Ebeling et al. 1996) in the Southern hemisphere. These catalogs are uncontaminated by non-cluster X-ray sources (AGNs or foreground stars). The BCS is 90% complete for fluxes higher than  $4.4 \times 10^{-12} \text{ erg cm}^{-2} \text{ s}^{-1}$  in the 0.1-2.4 keV band. The eBCS extends the BCS down to  $2.8 \times 10^{-12} \text{ erg cm}^{-2} \text{ s}^{-1}$  with 75% completeness. Finally,

the XBACS is an essentially complete sample of Abell clusters with fluxes above  $5.0 \times 10^{-12} \text{ erg cm}^{-2} \text{ s}^{-1}$ <sup>1</sup>.

The original W INGS sample comprises all clusters from BCS, eBCS and XBACS with a high Galactic latitude ( $|b| > 20$  deg) in the redshift range  $0.04 < z < 0.07$ . The redshift cut and the Galactic latitude are thus the only selection criteria applied on the X-ray samples. The redshift range has been chosen to guarantee both a large area coverage (the side of our field is  $34^{\circ} \times 1.6 \text{ Mpc}$ ) and sufficient spatial resolution ( $1^{\circ} \times 1.3 \text{ kpc}$ ) for all clusters.

After having removed the cluster A3391, because of the presence of strong non-uniform illumination in the CCD frames, the final W INGS sample includes 77 clusters (41 in the Southern hemisphere and 36 in the Northern one, see Figure 1), of which 18 in common with Dressler's (1980) sample. This partial overlap is useful to compare the two datasets and the morphological classifications. Table 1 lists the cluster name, coordinates of the adopted center, redshift, Abell richness, Bautz-Morgan type, X-ray luminosity in units of  $10^{44} \text{ erg s}^{-1}$ , color excess E(B-V) and cluster velocity dispersion from the literature (see notes on the Table).

The W INGS clusters span a wide range in X-ray luminosities ( $\log L_x [0.1-2.4 \text{ keV}] = 43.5-45.0$ ), corresponding to gravitational masses  $10^{14}$  to  $> 2 \times 10^{15}$  (Reiprich & Böhringer 2002), as well as in optical properties such as Abell richness and Bautz-Morgan type (see Figure 2).

### 4. W INGS-OPT Observations

The observations of the W INGS-OPT survey have been taken in dark time with the Wide Field Camera (WFC) mounted at the corrected f/3.29 prime focus of the INT-2.5m telescope in La Palma (Canary Islands, Spain) and with the Wide Field Imager (WFI) mounted at the f/8 Cassegrain focus of the MPG/ESO-2.2m telescope in La Silla (Chile) for the northern and southern clusters, respectively. The northern campaign consisted of three runs, for a total of 9 nights with 46 observed clusters. The southern campaign has produced data for 35 clusters during three observing runs (the last two in service mode), for a total of 2 nights in observer mode, plus about 48 hours of science exposures in service mode. Tables 2 and 3 list the observing runs of the W INGS-OPT survey and the main instrumental characteristics of the wide-field cameras, respectively.

#### 4.1. Survey requirements

Among the attributes of any photometric galaxy survey, the most important ones concern the spatial resolution and the photometric depth. Concerning the former,

<sup>1</sup> Note that our sample largely overlaps with the one studied by Smith et al. (2004). The data obtained are however complementary, since these authors have obtained B and R imaging and fiber spectroscopy of early-type red galaxies at a resolution higher than W INGS-SPE and suitable for galaxy velocity dispersion measurements.

Cluster	(J2000)		Redshift	Abell Rich.	B-M Type	$L_x = 10^{44}$ ergs s <sup>-1</sup>	E (B-V) mag	km / s
A 0085	00 41 50	-09 18	0.0521	1	I	8.38	0.038	749 (a)
A 0119	00 56 21	-01 15	0.0444	1	II-III	3.23	0.038	778 (a)
A 0133	01 02 42	-21 52	0.0603	0	-	3.57	0.018	623 (a)
A 0147	01 08 12	02 11	0.0447	0	III	0.54	0.025	-
A 0151	01 08 51	-15 24	0.0536	1	II	1.01	0.026	715 (a)
A 0160	01 13 04	15 30	0.0442	0	III	0.38	0.086	572 (a)
A 0168	01 15 09	00 17	0.0448	2	II-III	1.09	0.035	581 (a)
A 0193	01 25 07	08 41	0.0485	1	II	1.54	0.051	1136 (a)
A 0311	02 09 28	19 46	0.0657	0	-	0.81	0.174	-
A 0376	02 46 04	36 54	0.0488	0	I-II	1.39	0.073	-
A 0500	04 38 52	-22 06	0.0670	1	III	1.42	0.050	-
A 0548b	05 45 28	-25 55	0.0441	1	III	0.30	0.029	-
A 0602	07 53 26	29 21	0.0621	0	III	1.12	0.057	-
A 0671	08 28 32	30 25	0.0503	0	II-III	0.89	0.047	994 (a)
A 0754	09 08 32	-09 37	0.0542	2	I-II	8.01	0.064	880 (a)
A 0780	09 18 06	-12 05	0.0565	0	-	6.63	0.045	-
A 0957	10 13 38	-00 55	0.0448	1	I-II	0.78	0.042	678 (a)
A 0970	10 17 34	-10 40	0.0595	1	III	1.50	0.054	-
A 1069	10 39 43	-08 41	0.0622	0	III	0.95	0.041	-
A 1291	11 32 21	55 58	0.0527	1	III	0.44	0.019	919 (a)
A 1631a	12 52 52	-15 24	0.0466	0	I	0.73	0.054	-
A 1644	12 57 11	-17 24	0.0475	1	II	3.52	0.072	991 (a)
A 1668	13 03 46	19 16	0.0634	1	II	1.59	0.032	-
A 1736	13 27 11	-27 12	0.0461	-	III	2.37	0.058	381 (a)
A 1795	13 48 52	26 35	0.0622	2	I	11.12	0.013	896 (a)
A 1831	13 59 15	27 58	0.0612	1	III	1.90	0.019	-
A 1983	14 52 59	16 42	0.0444	1	III	0.47	0.027	504 (a)
A 1991	14 54 31	18 38	0.0586	1	I	1.35	0.033	510 (a)
A 2107	15 39 39	21 46	0.0411	1	I	1.10	0.057	536 (a)
A 2124	15 44 59	36 06	0.0654	1	I	1.36	0.025	852 (a)
A 2149	16 01 35	53 55	0.0675	0	-	0.83	0.010	-
A 2169	16 14 09	49 09	0.0579	0	III	0.45	0.015	-
A 2256	17 03 35	78 38	0.0581	2	II-III	7.05	0.053	1270 (a)
A 2271	17 18 17	78 01	0.0584	0	I	0.63	0.042	460 (a)
A 2382	21 51 55	-15 42	0.0644	1	II-III	0.91	0.057	-
A 2399	21 57 13	-07 50	0.0582	1	III	1.00	0.039	-
A 2415	22 05 40	-05 36	0.0590	0	III	1.69	0.066	-
A 2457	22 35 41	01 29	0.0591	1	I-II	1.43	0.084	-
A 2572a	23 17 13	18 42	0.0422	0	III	1.02	0.051	-
A 2589	23 23 57	16 46	0.0416	0	I	1.86	0.030	500 (a)
A 2593	23 24 20	14 38	0.0428	0	II	1.15	0.044	-
A 2622	23 35 01	27 22	0.0613	0	II-III	1.07	0.057	-
A 2626	23 36 30	21 08	0.0565	0	I-II	1.95	0.063	681 (a)
A 2657	23 44 57	09 11	0.0400	1	III	1.60	0.126	667 (a)
A 2665	23 50 50	06 09	0.0562	0	-	1.90	0.080	-
A 2717	00 03 13	-35 56	0.0498	0	I-II	1.01	0.011	537 (d)
A 2734	00 11 22	-28 51	0.0624	0	III	2.55	0.017	631 (d)
A 3128	03 30 15	-52 32	0.0590	-	I-II	2.12	0.016	854 (b)
A 3158	03 43 09	-53 39	0.0590	-	I-II	5.31	0.015	977 (d)
A 3164	03 45 49	-57 02	0.0611	0	I-II	1.48	0.027	-
A 3266	04 31 13	-61 27	0.0545	-	I-II	6.15	0.020	1120 (b)
A 3376	06 00 41	-40 02	0.0464	0	I	2.48	0.052	780 (b)
A 3395	06 27 36	-54 26	0.0497	0	II	2.80	0.113	1345 (b)
A 3490	11 45 20	-34 26	0.0697	2	I	1.72	0.087	-
A 3497	12 00 04	-31 23	0.0609	0	I-II	1.45	0.072	-
A 3528a	12 54 35	-29 23	0.0535	0	II	1.33	0.078	969 (e)
A 3528b	12 54 00	-28 51	0.0535	0	-	1.98	0.078	-
A 3530	12 55 36	-30 20	0.0544	0	I-II	0.87	0.086	391 (c)

Table 1. The WINGS cluster sample. References for are: (a) Struble & Rood 1991, (b) Struble & Ftaclas 1994, (c) Wu et al. 1998, (d) Makhdavi & Geller 2001, (e) Mazure et al. 1996, (f) Mulchaey et al. 2003

Cluster	(J2000)		redshift	Abell Rich.	B-M Type	$L_x = 10^{44}$ ergs s <sup>-1</sup>	E (B-V) mag	km/s
A 3532	12 57 21	-30 21	0.0555	0	II-III	2.83	0.085	742 (b)
A 3556	13 24 07	-31 40	0.0490	0	I	0.94	0.060	575 (d)
A 3558	13 27 57	-31 29	0.0477	-	I	6.27	0.050	737 (c)
A 3560	13 31 53	-33 14	0.0470	3	I	1.32	0.056	-
A 3562	13 33 35	-31 40	0.0502	2	I	3.33	0.058	736 (c)
A 3667	20 12 27	-56 49	0.0530	-	I-II	8.76	0.049	1510 (b)
A 3716	20 51 30	-52 43	0.0448	1	I-II	1.01	0.037	854 (b)
A 3809	21 46 59	-43 53	0.0631	-	III	2.25	0.018	479 (d)
A 3880	22 27 55	-30 34	0.0570	0	II	1.86	0.015	851 (d)
A 4059	23 57 00	-34 45	0.0480	1	I	3.09	0.017	903 (d)
IIIZW 108	21 13 56	02 33	0.0483	-	-	2.19	0.070	-
M KW 3s	15 21 52	07 42	0.0453	0	-	2.68	0.035	610 (c)
RX J0058	00 58 55	26 57	0.0470	-	-	0.44	0.068	674 (f)
RX J1022	10 22 10	38 31	0.0534	-	-	0.35	0.018	-
RX J1740	17 40 31	35 39	0.0430	-	-	0.50	0.026	-
ZwC 11261	07 16 41	53 23	0.0644	-	-	0.81	0.092	-
ZwC 12844	10 02 36	32 42	0.0500	-	-	0.57	0.015	-
ZwC 18338	18 10 50	49 55	0.0473	-	-	0.79	0.043	-
ZwC 18852	23 10 30	07 35	0.0400	-	-	0.94	0.065	-

Table 1. The W INGS cluster sample (continue)

WFC@INT -2.5m (North)					
Run number	PATT/CAT REF.	Starting Date	Alloc. Time	B Filtr.ID	V Filtr.ID
1	C3	Aug. 28, 2000	1 night	Harris (191)	Harris (192)
2	ITP3	Apr. 25, 2001	5 nights	Kitt Peak (210)	Harris (192)
4	ITP3	Sep. 15, 2001	3 nights	Harris (191)	Harris (192)
WFM PG/ESO -2.2m (South)					
Run number	Proposal ID	Starting Date	Alloc. Time	B Filtr.ID	V Filtr.ID
3	67A-0030	Aug. 15, 2001	2 nights	ESO 99 (842)	ESO 89 (843)
5	68A-0139	Feb. 14, 2002	30 hrs	ESO 99 (842)	ESO 89 (843)
6	69A-0119	Apr. 01, 2002	18 hrs	ESO new B (878)	ESO 89 (843)

Table 2. The W INGS-OPT observing runs

Feature	WFC@INT	WFM PG
Field of view	34° 34°	34° 33°
Pixel scale	0.3300/pixel	0.23800/pixel
Detector	4 2k 4k	8 2k 4k
Filling factor	93.6%	95.9%
Read-out time	37 sec.	27 sec.
Read-out noise (Inverse) gain	6.2 e-/pix	4.5 e-/pix
Full-well capacity	2.8 e- =ADU	2.0 e- =ADU
Telescope aperture	180,000 e	> 200,000 e
Telescope focus	2.54 m	2.20 m
	Prime focus	Cassegrain

Table 3. Technical features of the wide-field cameras used by the W INGS-OPT survey

Figure 3 shows the distribution of effective diameters (in Kpc) for early-type galaxies in the nearby clusters studied by Fasano et al. (2002). Since a good galaxy profile restoration is usually possible down to effective diameters of the order of the Full Width Half Maximum (FWHM)

of the point spread function (see Figure 4 in Fasano et al. 2002), we chose as the W INGS-OPT imaging requirement that the FWHM not exceed 1.5 kpc in our cosmological framework (the dotted line in Figure 3).

Concerning the photometric depth, our interest is twofold: First, we want the W INGS-OPT survey to be able to sample the luminosity function of clusters down to the dwarf galaxies ( $M_v = -14$ ). Second, we require that the depth is sufficient to allow a reliable surface photometry (S/N ratio 4.5 per square arcseconds) down to a surface brightness of  $v = 25$  mag arcsec<sup>-2</sup>. With the average (dark time) observing conditions at both WFC@INT and WFM PG, it turns out that this photometric depth can be fulfilled with exposure times of the order of 20-25 minutes, depending on the photometric band (see Sec. 4.2).

Sec. 8 illustrates to what extent the above mentioned requisites have been fulfilled by the W INGS-OPT observations.

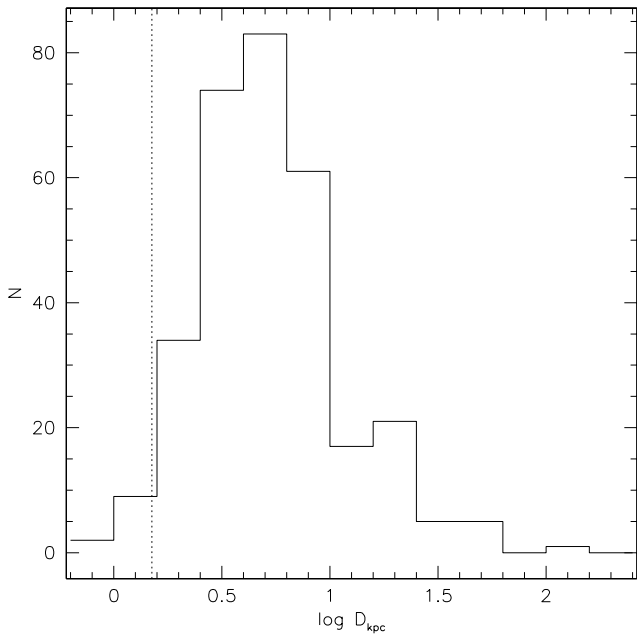


Fig. 3. Distribution of effective diameters (in Kpc) for early-type galaxies in the nearby clusters studied by Fasano et al. (2002). The dotted line corresponds to 1.5 Kpc

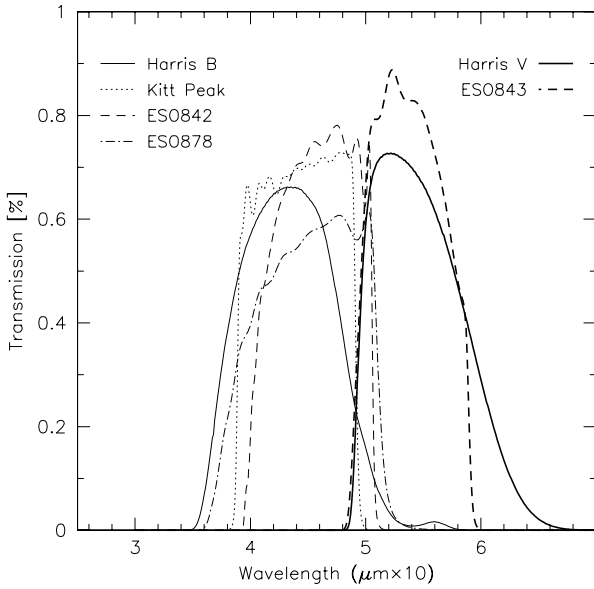


Fig. 4. Transmission curves of the filters used in the W INGS-OPT survey

#### 4.2. Observing strategy and outcome

We decided to take images in the V and B bands. The V filter allows us to compare our results with previous studies of nearby clusters, as well as with WFC2/ACS@HST (F814W) studies of clusters at  $z = 0.5$ . The B filter is

needed in order to get colors of galaxies and especially useful because it is the rest-frame equivalent to the imaging of clusters at  $z = 0.5$  done using HST + ACS. Table 2 reports the identifications of the broad band filters B and V used in the different W INGS-OPT observing runs, while in Figure 4 the transmission curves of the different filters are shown.

In order to avoid saturation of the brightest objects, usually three exposures per filter have been obtained, also allowing us to easily remove cosmic rays. For A 3528b (run # 5) we have just one exposure per filter (3m and 8m in the B and V band, respectively).

We aimed for similar FWHM for each of the summed exposures. Thus, whenever possible we tried to take these exposures with a short interval between them. Obviously, this was not always the case for clusters observed in service mode (runs # 5 and # 6 with WFPC2/MPG). In particular, for nine clusters observed during the run # 6 (A 2382, A 2399, A 2717, A 2734, A 3667, A 3716, A 3809, A 3880 and A 4059), we got from ESO two medium seeing, long exposures and a good seeing, short exposure per filter. In a forthcoming paper of the series we will exploit this occurrence to check the dependence of the surface photometry on the seeing.

During the first observing run we explored with a single cluster (A 2107) the possibility of taking three shifted exposures per filter in order to fully sample the gaps between CCDs. After mosaicing, however, we verified that, due to the worsening of the S/N ratio within the underexposed regions, this procedure resulted in a net loss of the area usable to perform a deep surface photometry. Thus, we decided to abandon this technique. Instead, during the whole run # 4 and for many clusters observed in service mode during the runs # 5 and # 6, a small shifting in right ascension (25 pix.) was applied allowing us to remove bad pixels and columns.

In order to provide the W INGS-OPT survey with accurate astrometric solutions and background galaxy counts estimation for both WFPC2/INT and WFPC2/MPG cameras, we have also imaged the astrometric regions ACR-D/E/M/N from Stone et al. (1999) and a blank field in each hemisphere.

Finally, some dark and dome flat exposures and several bias frames, twilight sky-frames and photometric standard fields have been obtained for each observing night.

Table 4 reports the observing log of the W INGS-OPT survey.

#### 5. Image reduction

Most of the steps required to reduce the data coming from mosaic wide-field cameras are similar to those usually performed on traditional CCD frames, but the use of such a wide area mosaic raises a number of new technical issues, mainly related to the presence of geometric distortions and photometric differences between the different CCDs. In addition, handling the huge amount of pixels from this

Cluster	Run	Night	V band					B band				
			# exp	T <sub>exp</sub>	sky	fw hm "	m lim	# exp	T <sub>exp</sub>	sky	fw hm "	m lim
A 85	4N	15-Sep-01	3	400	21.16	1.25	24.12	3	420	22.17	1.27	24.68
A 119	4N	15-Sep-01	3	400	21.32	1.20	24.29	3	420	22.23	1.30	24.66
A 133	3S	15-Aug-01	3	460	21.56	1.14	23.84	3	420	22.36	1.38	24.06
	6S	12-Jul-02	2	540	21.27	1.45	22.99	2	480	22.04	1.40	23.73
A 147	1N	28-Aug-00	3	400	21.36	1.15	24.34	3	420	22.07	1.08	24.89
	4N	17-Sep-01	3	400	21.25	1.25	24.16	3	420	22.22	1.24	24.75
A 151	4N	16-Sep-01	3	400	21.13	1.10	24.31	3	420	22.14	1.30	24.51
A 160	4N	16-Sep-01	3	400	21.23	1.10	24.42	3	420	22.23	1.12	24.95
A 168	1N	28-Aug-00	3	400	21.37	1.20	24.25	3	420	22.21	1.16	24.80
A 193	1N	28-Aug-00	3	400	21.33	1.55	23.67	3	420	22.18	1.50	24.23
	4N	17-Sep-01	3	400	21.29	1.18	24.36	3	420	22.37	1.23	24.95
A 311	4N	15-Sep-01	3	400	21.42	1.20	24.34	3	420	22.32	1.23	24.82
A 376	4N	16-Sep-01	3	400	21.39	1.30	24.10	3	420	22.33	1.36	24.54
A 500	5S	17-Feb-02	3	460	21.48	1.00	23.98	3	420	22.15	1.05	24.39
A 548b	5S	17-Feb-02	3	460	21.29	1.00	23.89	3	420	22.13	1.05	24.38
A 602	2N	26-Apr-01	3	400	20.78	1.20	24.02	3	420	21.60	1.33	24.38
A 671	2N	26-Apr-01	3	400	20.90	1.30	23.90	3	420	21.81	1.30	24.53
A 754	2N	27-Apr-01	3	400	20.65	1.27	23.84	3	420	21.43	1.25	24.43
A 780	2N	29-Apr-01	3	400	20.15	1.90	22.70	3	420	20.35	1.75	23.17
	6S	07-Apr-02	3	460	21.20	1.21	23.50	3	420	22.14	1.12	24.42
A 957	2N	28-Apr-01	3	400	20.68	1.43	23.58	3	420	21.21	1.73	23.62
A 970	2N	28-Apr-01	3	400	20.53	1.43	23.51	3	420	20.87	1.50	23.67
	6S	03-Apr-02	3	460	20.15	1.24	22.93	3	420	20.39	1.20	23.42
A 1069	2N	27-Apr-01	3	400	20.76	1.30	23.84	3	420	21.30	1.38	24.06
A 1291	2N	29-Apr-01	3	400	20.85	1.30	23.87	3	420	21.47	1.34	24.30
A 1631a	5S	15-Feb-02	3	460	20.99	0.85	24.14	3	420	21.81	1.12	24.16
A 1644	5S	15-Feb-02	3	460	21.00	0.71	24.54	3	420	21.82	0.81	24.87
A 1668	2N	25-Apr-01	3	600	21.02	1.55	23.80	3	600	22.04	1.40	24.70
A 1736	5S	15-Feb-02	3	460	21.18	0.74	24.53	3	420	21.94	0.83	24.88
A 1795	2N	26-Apr-01	3	400	21.32	1.00	24.68	3	420	22.41	1.03	25.34
A 1831	2N	25-Apr-01	3	400	21.12	1.33	23.96	3	600	22.13	1.20	25.08
A 1983	2N	26-Apr-01	3	400	21.38	0.93	24.87	3	420	22.43	0.96	25.49
A 1991	2N	26-Apr-01	3	400	21.37	1.03	24.64	3	420	22.44	1.00	25.41
A 2107	1N	28-Aug-00	3	400	21.22	1.05	24.46	3	420	22.16	1.23	24.66
A 2124	2N	25-Apr-01	3	400	21.08	1.03	24.50	3	420	22.01	1.38	24.52
A 2149	2N	27-Apr-01	3	400	19.79	1.00	23.32	3	420	21.08	1.10	24.03
A 2169	4N	16-Sep-01	3	400	21.25	1.10	24.45	3	420	22.36	1.80	23.98
A 2256	2N	25-Apr-01	3	400	21.12	1.21	24.17	3	420	22.33	1.20	24.97
A 2271	2N	27-Apr-01	3	400	19.96	1.20	23.13	3	420	20.95	1.15	23.86
A 2382	6S	12-Jun-02	2	540	21.11	1.24	23.27	2	480	21.85	1.40	23.64
	6S	13-Jul-02	1	300	21.37	1.05	23.02	1	300	22.08	0.88	24.12
A 2399	6S	12-Jun-02	2	540	21.12	1.40	23.01	2	480	21.87	1.52	23.47
	6S	13-Jul-02	1	300	21.43	1.20	22.76	1	300	22.13	1.00	23.86
A 2415	1N	28-Aug-00	3	400	21.04	1.45	23.68	3	420	21.99	1.23	24.57
A 2457	4N	17-Sep-01	3	400	21.11	1.35	23.92	3	420	22.13	1.31	24.59
A 2572a	4N	17-Sep-01	3	400	21.33	1.20	24.29	3	420	22.29	1.28	24.72
A 2589	1N	28-Aug-00	3	400	21.46	1.70	23.54	3	420	22.29	1.65	24.08
	4N	17-Sep-01	3	400	21.21	0.85	24.98	3	420	22.18	0.98	25.24
A 2593	1N	28-Aug-00	3	400	21.42	2.05	23.11	3	420	22.22	1.60	24.11
	4N	17-Sep-01	3	400	21.18	0.95	24.72	3	420	22.20	1.05	25.11
A 2622	4N	15-Sep-01	3	400	21.29	1.23	24.22	3	420	22.28	1.26	24.75
A 2626	1N	28-Aug-00	3	400	21.49	1.64	23.63	3	420	22.30	1.73	23.98
A 2657	4N	16-Sep-01	3	400	21.29	1.35	24.02	3	420	22.20	1.31	24.60
A 2665	4N	17-Sep-01	3	400	21.16	1.04	24.51	3	420	22.12	1.16	24.85
A 2717	3S	15-Aug-01	3	460	21.69	1.33	23.57	3	420	22.44	1.45	23.99
	6S	13-Jun-02	2	540	20.48	1.34	22.86	2	480	22.26	1.28	24.14
	6S	13-Jul-02	1	300	21.32	0.75	23.73	1	300	22.19	0.90	24.12
A 2734	6S	13-Jun-02	2	540	21.33	1.45	23.10	2	480	22.14	1.22	24.19
	6S	14-Jul-02	1	300	21.48	1.12	22.94	1	300	22.23	1.05	23.80
A 3128	5S	16-Feb-02	3	460	21.29	1.50	23.05	3	420	22.00	1.33	23.88

Table 4. The W INGS-OPT observing log.

Cluster	Run	Night	V band					B band				
			# exp	T <sub>exp</sub>	sky	fw hm "	m lim	# exp	T <sub>exp</sub>	sky	fw hm "	m lim
A 3158	5S	17-Feb-02	3	460	21.44	1.38	23.31	3	420	21.93	1.10	24.26
A 3164	5S	15-Feb-02	3	460	21.42	1.22	23.56	4	420	22.13	1.62	23.67
A 3266	5S	16-Feb-02	3	460	21.22	1.07	23.75	3	420	21.99	1.17	24.15
A 3376	5S	15-Feb-02	3	460	21.14	1.14	23.53	3	420	21.94	1.19	24.01
A 3395	5S	17-Feb-02	3	460	21.11	0.90	24.03	3	420	21.84	0.85	24.70
A 3490	5S	16-Feb-02	3	460	20.92	1.15	23.45	3	420	21.73	1.07	24.22
A 3497	5S	17-Feb-02	3	460	21.39	0.69	24.79	3	420	22.10	0.69	25.36
A 3528a	5S	15-Feb-02	3	460	20.91	0.83	24.15	3	420	22.03	0.86	24.84
A 3528b	5S	15-Feb-02	1	460	21.38	0.83	23.79	1	180	22.09	0.92	23.63
A 3530	5S	16-Feb-02	3	460	20.99	1.06	23.66	3	420	21.80	1.06	24.27
A 3532	5S	16-Feb-02	3	460	21.21	0.90	24.12	3	420	21.95	0.95	24.59
A 3556	5S	16-Feb-02	3	460	21.33	0.83	24.36	3	420	22.08	0.83	24.94
A 3558	5S	17-Feb-02	3	460	21.35	0.86	24.29	3	420	21.98	0.87	24.80
A 3560	5S	17-Feb-02	3	460	21.40	0.83	24.39	3	420	22.06	0.86	24.86
A 3562	5S	16-Feb-02	1	180	21.31	0.86	23.14	1	180	22.01	0.95	23.53
A 3667	6S	12-Jun-02	2	540	21.39	1.60	22.84	2	480	22.19	1.75	23.33
	6S	13-Jul-02	1	300	21.57	1.10	23.02	1	300	22.28	1.00	23.93
A 3716	6S	12-Jun-02	2	540	21.33	1.65	22.75	2	480	22.19	1.50	23.66
	6S	13-Jul-02	1	300	21.58	1.15	22.92	1	300	22.32	1.15	23.64
A 3809	6S	12-Jun-02	2	540	21.24	1.50	22.91	2	480	22.07	1.38	23.79
	6S	13-Jul-02	1	300	21.55	1.12	22.97	1	300	22.30	1.10	23.73
A 3880	3S	15-Aug-01	3	460	21.63	1.45	23.35	3	420	22.38	1.38	24.07
	6S	13-Jun-02	2	540	21.20	1.47	22.94	2	480	22.00	1.21	24.04
	6S	13-Jul-02	1	300	21.28	1.02	23.05	1	300	22.11	1.26	23.35
A 4059	6S	13-Jun-02	2	540	21.14	1.33	23.12	2	480	21.97	1.25	23.95
	6S	13-Jul-02	1	300	21.41	0.75	23.78	1	300	22.22	0.95	24.02
IZW 108	4N	15-Sep-01	3	400	21.23	1.60	23.62	3	420	22.15	1.68	24.06
	4N	17-Sep-01	4	400	21.25	1.25	24.32	-	-	-	-	-
M KW 3S	2N	27-Apr-01	3	400	19.87	1.11	23.26	3	420	21.21	1.16	24.12
RX J0058	4N	16-Sep-01	3	400	21.51	1.20	24.37	3	420	22.44	1.13	25.02
RX J1022	2N	27-Apr-01	3	400	20.86	1.10	24.25	3	420	21.84	1.16	24.79
RX J1740	2N	26-Apr-01	3	400	21.48	1.10	24.55	3	420	22.53	1.15	25.15
ZwC 11261	4N	15-Sep-01	3	400	21.14	1.08	24.43	3	420	22.20	1.26	24.71
ZwC 12844	2N	27-Apr-01	3	400	20.77	1.03	24.35	3	420	21.72	1.06	24.93
ZwC 18338	2N	26-Apr-01	3	400	21.52	1.03	24.72	2	420	22.38	1.13	24.90
	2N	28-Apr-01	1	400	21.24	1.55	23.09	1	420	22.25	1.45	23.92
ZwC 18852	4N	15-Sep-01	3	400	21.08	1.36	23.90	3	420	22.02	1.43	24.35

Table 4. The W INGS-OPT observing log (continue).

kind of detectors requires that even the standard reduction procedures must be revised, to make them more efficient.

The whole reduction procedure has been carried out by means of IRAF-based tools. In particular, specially designed IRAF scripts have been assembled to produce automatically super-bias and super-at frames for each observing night (Marmo 2003). The specific tasks related to the treatment of wide-field imaging (astrometry and mosaicing), even with the particular layout of the WFC@INT camera, have been managed by the IRAF mosaic reduction package MSCRED (Valdes 1998) and the IRAF script package WFPRED developed at the Padova Observatory (Rizzi and Held, private communication).

The dark current turned out to be always negligible for both WFC@INT and WFI@MPG cameras and was not considered in the reduction pipeline. Similarly, we have not applied fringing correction, since no significant fringe

patterns are found in both B and V frames for either WFC@INT and WFI@MPG.

### 5.1. Bias removal

The bias frames of the WFC@INT camera showed some significant low frequency structure, with slight systematic differences among different nights, thus, a 2D bias removal was required. To produce a reliable and almost noiseless bias frame for each night (super-bias), we used a specially designed, automatic IRAF procedure comparing mean, standard deviation and skewness of the different bias frames and combining only the ones showing homogeneous trends. The average scatter of the super-bias counts turned out to be negligible (0.5–0.8 ADU per pixel: 7 magnitudes below the sky surface brightness). We applied

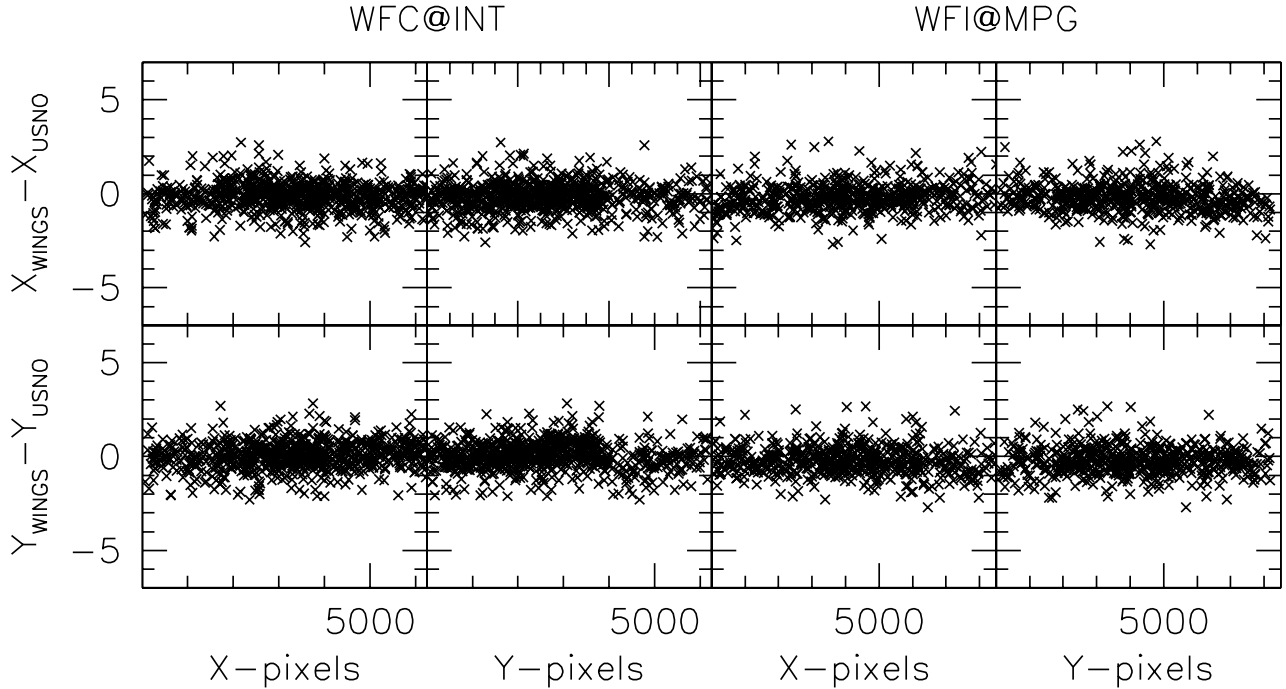


Fig. 5. X-pix and Y-pix differences between WINGS and USNO coordinates of galaxies, after having applied our astrometric solutions for WFC@INT (left) and WFI@MPG (right).

the same procedure to WFI@MPG images, although in this case the bias frames showed more constant patterns.

### 5.2. Linearity correction

Specific tests revealed that the CCDs of the WFC@INT camera suffer from significant nonlinearities over the whole dynamic range. These have been corrected according to the prescriptions given in the CASU INT Wide Field Survey page (<http://www.ast.cam.ac.uk/wfcsur/foibles.htm>). In order to allow the correction to be performed automatically, the coefficients of the equations given there have been included in the headers of WFC images. No linearity problems have been found in the WFI@MPG detectors.

### 5.3. Flat fielding

Domestic flats turned out to be much less stable than sky-flats and were never used. Again, night super-flats have been produced by an automatic IRAF script we have devised for this purpose. After bias subtraction, linearity correction and trimming of the flats, this procedure rejected the low (counts and close-to)saturation flats; then a single, normalized super-flat was produced for each filter, combining those flats whose marginal distributions of counts along both the X and the Y axes had similar values of mean, standard deviation and skewness. Both the random (pixel by pixel) variance and the systematic dif-

ferences among flats taken in the same nights turned out to be less than 1% (0.01 mag). Sky flats taken in different nights of the same observing run usually showed a good agreement among each other, while significant differences have been found in the patterns of flats taken in different runs.

Due to non uniform illumination, the WFI@MPG camera has been reported to show significant large-scale spatial gradients in photometry across the entire field of view, and across each of its eight chips individually (Manfroid et al. 2001; Koch et al. 2003). This problem cannot be solved by usual flat fielding because the illumination unevenness affects in the same manner both flats and science exposures. We will report about that in Sec. 6.

### 5.4. Astrometry

Finding an astrometric solution adequate to the proposed scientific objectives is a specific and critical task to be addressed when dealing with wide-field imaging. Usually, the wider the field, the larger the geometric distortions introduced by the optical layout of the camera. It is important to note that, besides the astrometric measurements, such distortions can also significantly affect the photometric ones, due to the misshaped smearing of the light on the pixel array. In order to map, model and correct distortions in wide-field images one has to compare physical (pixels) and world (, ) coordinates for a given sample of point-like sources (stars) in the field. Strong distortions require

sizeable astrometric samples of stars uniformly spread along the field. Since such samples are seldom available, it is often convenient to adopt an astrometric solution obtained only once for all from a suitable astrometric field containing several hundreds (or even thousands) of stars.

The WFC@INT imaging is well known to be affected by strong geometrical distortions. The astrometric solutions for the two filters B and V have been obtained using the astrometric regions ACR-D and ACR-N (Stone et al. 1999) and the wfpred.wfpastro task. These solutions have been applied (after re-centering with wfpred.wfpzero) to each northern cluster and standard field using the task wfpred.wfpsetwcs.

For the WFI@MPG camera, a precise wfpred astrometric solution, obtained using the astrometric regions ACR-E and ACR-M (Stone et al. 1999), was already available (Rizzi and Held, private communication). In this case, only the re-centering step was performed.

Figure 5 shows the differences (in pixel units) between WINGS and USNO (Monet, 1998) coordinates of galaxies for three clusters observed with WFC@INT (A 85, A 119, A 168; left panels) and three more clusters observed with WFI@MPG (A 500, A 3395, A 3490; right panels). The comparison is performed using galaxies since the stars of the USNO database are usually saturated in our imaging. Since centering algorithms are likely much less precise for galaxies than for stars, the formal precision obtained from the astrometric solution applied to the stars of the astrometric fields (rms: 0.1 pix) turns out to be much smaller than the one found for galaxies and shown in Figure 5 (rms: 0.75 pix, corresponding to 0.25 and 0.18 arcseconds in the case of WFC@INT and WFI@MPG, respectively). Still, this is accurate enough to ensure a precise pointing for the multi-fiber spectroscopy carried out with both WYFFOS@WHT (fiber of 1.6 arcseconds) and 2dF@AAT (fiber of 2.1 arcseconds).

## 6. Photometric Calibration

Since the CCDs of any mosaic camera have usually different zero points and color responses, the optimal standard fields for WFI imaging should map each CCD with a sufficient number of stars covering wide ranges of both magnitude and color. For this reason, the problem of photometric calibration in wide-field CCD mosaics cameras is not yet solved satisfactorily. Nowadays there are two main sets of standard fields that, even if they not provide a complete coverage of the CCD mosaic, can be used satisfactorily for wide-field photometry, namely the sample of Landolt (1992) and that of Stetson (2000; see <http://cadcwww.hia.nrc.ca/cadcbin/wdbi.cgi/astrocatt/stetson/>). We preferred to use the Landolt sequences, since the Stetson's standard fields, even going deeper than the Landolt ones (typically fainter than 14th magnitude, with a larger number of standard stars), normally cover not more than 20 arcminutes by side. Actually, NGC 6633 was the only Stetson's standard field we used for our calibration (run # 4). We used the same set of Landolt's

fields through both the INT and the MPG observing runs, namely SA 92/95/98/101/104/107/110/113. During each night two or three SA fields were observed at different zenith distances in order to map the atmospheric extinction. However, the long average duration of each cluster pointing made difficult (often impossible) to observe the same standard field more than twice per night. In addition, the small number of stars usually present in the standard fields makes often insufficient (sometimes lacking) the photometric sampling of each CCD in a single calibration frame.

Thus, after having processed the standard fields with the usual steps (bias subtraction, linearity correction, trimming, astrophotometry and astrometry), we have performed the photometric calibration using a self-consistent method, taking advantage of all the standard fields in each observing run (Moles et al. 1985; see also Varela et al. 2004).

This method assumes that, even though the atmospheric extinction varies night by night, the observing set remains stable during each observing run. This implies that the out-of-atmosphere instrumental magnitude of each standard star measured on a given chip of the mosaic, is constant through the run, being different in different chips. Thus, for each observing run and for each

filter, this procedure provides us with an extinction coefficient for each night and with a set of zero points and color coefficients (one pair for each CCD of the mosaic) holding for the entire run.

First, we looked for the extinction coefficients, solving the following system of  $N$  generalized Bouguer's equations:

$$m_{scn} = m_{0,sc} + k_n X \quad ; \quad = 1, \dots, N \quad (1)$$

where  $k$  is the extinction coefficient,  $X$  is the airmass and  $N$  is the number of determinations ( $m$ ) obtained for the out-of-atmosphere instrumental magnitude ( $m_0$ ) of a given star ( $s$ ) during a given night ( $n$ ) in a given chip of the mosaic ( $c$ ).

For the sake of formal simplicity, in the minimization algorithm the equations (1) have been expressed in the form:

$$m_{scn} = m_{0,fp;qc} + \sum_{r} k_r X_r m_r; \quad (2)$$

where the indexes  $fp;qc$  respectively span all possible values of  $f$ ;  $c$ ;  $q$  and  $\delta$  is the Kronecker symbol. Table 5 shows the extinction coefficients obtained in this way for each filter in each observing night (see the table caption as far as the Run # 6 is concerned). Table 6 reports, for each observing run and for each filter, the photometric zero points  $Z_c$  and the color coefficients  $C_c$  of the different mosaics ( $c$ ). Each pair of coefficients is obtained solving a system of equations like this:

$$(m_{0,sc} \quad m_s^{std}) = Z_c + C_c \quad (B \quad V)_s^{std}; \quad (3)$$

where the out-of-atmosphere instrumental magnitudes  $m_{0,sc}$  are known from equations 2,  $m_s^{std}$  and  $(B \quad V)_s^{std}$

Run	Night	$k^V$	$k^B$
# 1	28-Aug-2000	0.115	0.198
# 2	25-Apr-2001	0.117	0.225
	26-Apr-2001	0.113	0.249
	27-Apr-2001	0.106	0.259
	28-Apr-2001	0.123	0.246
	29-Apr-2001	0.122	0.255
# 3	15-Aug-2001	0.116	0.179
	16-Aug-2001	0.118	0.188
# 4	15-Sep-2001	0.099	0.195
	16-Sep-2001	0.133	0.252
	17-Sep-2001	0.109	0.199
# 5	14-Feb-2002	0.091	0.158
	15-Feb-2002	0.092	0.159
	16-Feb-2002	0.086	0.147
# 6	Apr-Jul-2002	0.150	0.200
	Aug-2002	0.092	0.238

Table 5. Extinction coefficients of the W INGS-OPT survey. The extinction coefficients of the Run # 6 were fixed to the values given in the ESO web site because the scarcity of measurements made it impossible computing this values from the standard observations.

are the standard magnitudes and colors taken from the Landolt (1992) catalogs and  $c$  and  $s$  span all possible chips and stars, respectively.

During the Run # 6-Apr. (service mode) no standard stars were observed in the CCD # 8. We used for this run the  $Z_c$  and  $C_c$  coefficients of the Run # 6-June (also reported in Table 6). It is worth noticing, however, that the observations from Run # 6-Apr. (A 780 and A 970) have been just used to compare the photometry between WFC@INT and WFI@ESO (see Figure 13).

Figure 6 shows, for each observing run and for all observations of the standard stars, the residuals (given by eq. 3) of our photometric calibration in the two bands as a function of both standard magnitudes and colors. Excluding from the calibration set the saturated and blended stars and using a recursive  $k$  procedure to remove possible outliers, the total, typical rms of the residuals we achieved with our calibration is of the order of 0.02<sup>m</sup> (see Table 7).

Trying to disentangle the different contributions to the total scatter, we have analysed different nights of the same run. In Table 7, the right column relative to each filter reports the contribution to the scatter arising from sky transparency fluctuations through the run. In this turn, it may consist of a 'night contribution', a 'run contribution' and a 'long-term contribution' (the last one only for runs in service observing). These have been estimated normalizing the residuals relative to each individual star to their average values and using night-, run- and long-term base-lines, respectively. These contributions turn out to be roughly equivalent among each one another. From Table 7 it is clear that sky transparency variations do not represent the dominant contribution to the scatter in the photometric calibration. This must be due to systematic

Run	Chip (c)	$Z_c^V$	$C_c^V$	$Z_c^B$	$C_c^B$
# 1	1	24.61	-0.023	24.63	0.039
	2	24.61	-0.022	24.62	0.034
	3	24.57	-0.013	24.57	0.071
	4	24.60	-0.011	24.59	0.029
# 2	1	24.74	-0.001	25.00	0.093
	2	24.71	0.001	25.00	0.122
	3	24.70	0.016	24.98	0.136
	4	24.71	0.001	24.98	0.114
# 3	1	24.18	-0.072	24.73	0.162
	2	24.24	-0.114	24.72	0.192
	3	24.24	-0.149	24.70	0.186
	4	24.24	-0.059	24.72	0.202
	5	24.20	-0.073	24.69	0.259
	6	24.16	-0.066	24.65	0.251
	7	24.20	-0.092	24.66	0.214
	8	24.23	-0.056	24.71	0.221
# 4	1	24.76	-0.063	24.77	0.044
	2	24.70	0.020	24.78	0.031
	3	24.68	0.015	24.75	0.081
	4	24.71	-0.002	24.80	0.026
# 5	1	24.08	-0.079	24.51	0.278
	2	24.04	-0.069	24.51	0.239
	3	24.04	-0.067	24.46	0.311
	4	24.10	-0.078	24.52	0.282
	5	24.07	-0.038	24.50	0.273
	6	24.04	-0.085	24.48	0.249
	7	24.03	-0.082	24.47	0.259
	8	24.12	-0.103	24.58	0.247
# 6-Apr	1	24.19	-0.080	24.79	0.200
	2	24.18	-0.114	24.73	0.212
	3	24.17	-0.102	24.74	0.213
	4	24.21	-0.083	24.78	0.230
	5	24.17	-0.043	24.75	0.243
	6	24.13	-0.072	24.71	0.220
	7	24.12	-0.086	24.70	0.220
	8	24.13	-0.036	24.67	0.294
# 6-Jun	1	24.19	-0.083	24.80	0.183
	2	24.09	+ 0.032	24.73	0.220
	3	24.21	-0.133	24.77	0.201
	4	24.17	-0.037	24.76	0.243
	5	24.22	-0.138	24.77	0.200
	6	24.07	-0.023	24.69	0.215
	7	24.10	-0.049	24.67	0.268
	8	24.13	-0.036	24.67	0.294
# 6-Jul	1	24.16	-0.077	24.71	0.229
	2	24.10	-0.008	24.73	0.223
	3	24.09	-0.048	24.74	0.179
	4	24.15	-0.031	24.75	0.239
	5	24.16	-0.083	24.76	0.180
	6	24.08	-0.045	24.69	0.251
	7	24.09	-0.059	24.65	0.286
	8	24.11	-0.010	24.68	0.295
# 6-Aug	1	24.17	-0.176	24.87	0.090
	2	24.01	-0.041	24.70	0.271
	3	24.01	-0.054	24.70	0.242
	4	24.00	+ 0.025	24.69	0.341
	5	24.06	-0.090	24.72	0.214
	6	24.00	-0.081	24.67	0.231
	7	24.00	-0.078	24.55	0.370
	8	24.00	-0.002	24.59	0.334

Table 6. Calibration coefficients of the W INGS-OPT survey.

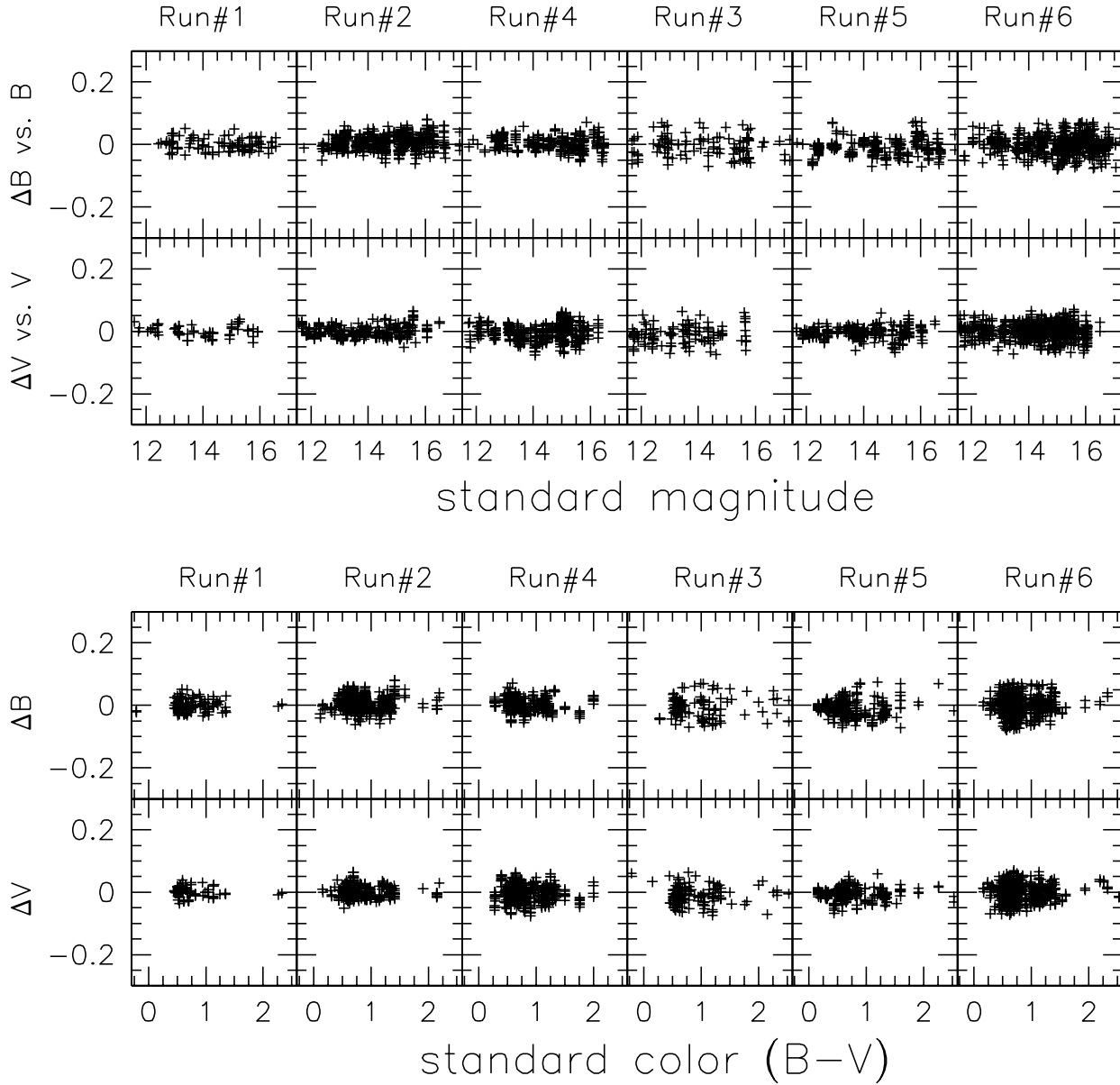


Fig. 6. Residuals of our photometric calibration for each observing run and for each band, as a function of both standard magnitudes and colors.

discrepancies likely arising both from possible zero point gradients through the fields and from the differences among photometric systems.

In Sec. 5.3 we reported about the non uniform illumination of the imaging taken with WFM PG, which can induce systematic magnitude differences up to 0.1 mag through the field. Even though our chip by chip photometric calibration procedure should in principle alleviate this problem, we have directly checked the un-uniformity of our photometric zero points by plotting in Figure 7 (left panels) the residuals of our calibration versus the pixel coordinates for the whole set of standard stars observed with WFM PG. Since in both filters a significant dependence

on the position is found to persist for the residuals, we have interpolated them through the field using a 2nd-order, 2D polynomial.

The right panels of Figure 7 show that the residuals after correction no longer depend on the position.

No significant spatial gradients of the residuals of the photometric calibration were found in the case of the WFC@INT camera. Tab. 8 summarizes the above mentioned, different contributions to the scatter, averaged over the whole data-set of standard stars observations available for each camera.

Run	B		V	
	Total	Sky Transp.	Total	Sky Transp.
# 1	0.020	0.010	0.017	0.007
# 2	0.023	0.014	0.018	0.007
# 4	0.022	0.009	0.026	0.014
# 3	0.034	0.020	0.028	0.016
# 5	0.026	0.016	0.023	0.013
# 6	0.030	0.022	0.026	0.018

Table 7. Total rms and sky transparency contribution to the rms of the residuals of the photometric calibration in the two bands for each observing run of the W INGS OPT survey.

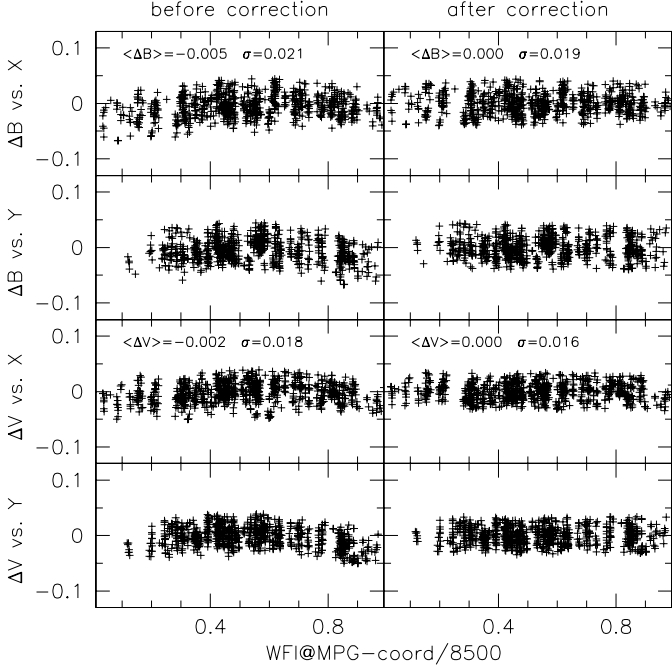


Fig. 7. Residuals of our calibration versus the pixel coordinates, for the whole set of standard stars observed with WFI@MPG, before (left panels) and after (right panels) correction

Cam era	W FC@INT		W FI@MPG	
	B	V	B	V
Sky Transp.	0.013	0.011	0.019	0.015
Phot.Syst.	0.018	0.020	0.018	0.016
ZP Gradient	-	-	0.010	0.010
Total	0.022	0.023	0.028	0.024

Table 8. Different contributions to the rms of the residuals of the photometric calibration in the two bands and for each W F camera

## 7. Mosaics and Catalogues

After having gone through the usual reduction procedure (de-biasing, linearity correction, astrometry), the multi-extension exposures of each given cluster in each

filter have been registered, co-added and mosaiced using the wfpc1.wfpcomb task.

Figures 8 and 9 show examples of the mosaics imaging obtained with the WFC@INT and WFI@MPG cameras, respectively. We produced co-added and mosaiced frames even when the different exposures of a given cluster came from different observing nights, with different observing conditions. However, in this cases, also the mosaics of just the exposures with coherent conditions were produced. For instance, when two medium seeing, long exposures and a good seeing, short exposure per filter were available (we clusters observed during run # 6; see Sec. 4), besides the co-added mosaic of the three exposures, we produced that of the two medium seeing exposures and the mosaic of the good seeing exposure. In fact, each one of them could be suitable for a particular task (integrated photometry, surface photometry, morphology).

In Sec. 7.3 we will see that the photometric quantities included in our catalogs are derived by running SExtractor (Bertin & Arnouts, 1996) over the co-added mosaics. In order to properly do that we had to further process them as follows.

First, each CCD of each multi-extension image has been divided by the exposure time and diminished by the mode of the histogram of the pixel counts, assumed to be a rough estimate of the average sky value. In Sec. 7.2 the final, much more accurate procedure we used for background subtraction is described. Provisionally, the outlined procedure provided a flat, close to zero background over the whole image, allowing us to perform the next step of the reduction procedure, that is the correction for both atmospheric extinction and gain differences among the different CCDs.

For each observing run and for each filter, this is obtained by multiplying each pixel of the mosaic image by the factor:

$$10^{0.4[(Z_c - Z) - k_n(\chi - 1)]} \quad (4)$$

where  $n$  and  $c$  are the night and the CCD which the pixel comes from, while  $Z$  and  $k_n$  represent the CCD-averaged zero point of the run and the extinction coefficient of the night, respectively. The newly derived image can be processed as a whole by SExtractor, using the virtual zero point:

$$Z_{\text{SEX}} = Z - k_n \quad (5)$$

Since the color terms of the photometric calibration are not considered in the outlined procedure, the magnitudes derived in this way by SExtractor ( $m_{\text{SEX}}$ ) have to be color-corrected afterwards, according to the true colors of the objects which they are referred to, as well as to the CCD ( $c$ ) where the objects are located in:

$$m = m_{\text{SEX}} + C_c (B - V) \quad (6)$$

In this formula  $C_c$  represents the color coefficient of the particular CCD and the true color ( $B - V$ ) can be easily evaluated by:

$$(B - V) = (B_{\text{SEX}} - V_{\text{SEX}}) / (1 - C_c) \quad (7)$$

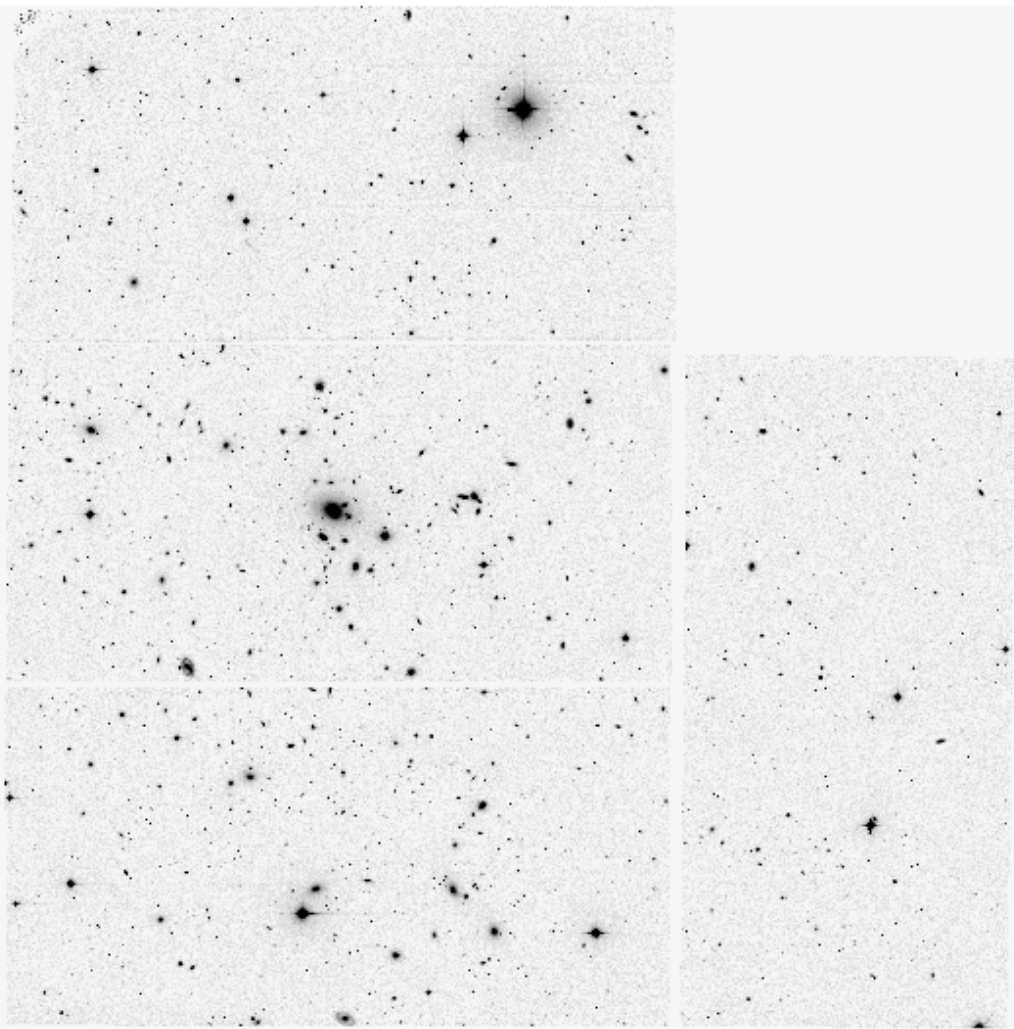


Fig. 8. Mosaic of the WFC@INT image of the cluster A 151. North is up, East is left.

$$\text{where } C_c = C_c^B - C_c^V.$$

The headers of the co-added mosaics frames of each cluster have been updated with keywords giving the proper photometric coefficients (including  $Z_{\text{SEX}}$  and  $C_c$ ) and the subtracted background values.

It is worth noticing that the mosaics frames obtained by co-addition of exposures taken in different observing nights (some clusters of run # 6), possibly with different calibration coefficients  $Z_c$  and  $C_c$ , in principle cannot be processed as explained above. The procedure we used in this case, that is to adopt weight-averaged calibration coefficients, is likely to be only a crude approximation. Therefore, even though these mosaics can be useful for surface photometry and morphology, they cannot be trusted as far as the absolute photometry is concerned.

### 7.1. Cosmics

Since for each cluster three exposures per filter with a short interval between them were usually obtained (see Sec. 4), the co-adding procedure was in general su-

cient to remove cosmic rays. When less than three close exposures were available we resorted to the IRAF tool COSMICRAYS to do the job.

For nearly half of the cluster sample (run # 4 and part of runs # 5 and # 6) the three available exposures were dithered of 25 pixels, allowing us to remove the bad pixels and columns. For the remaining clusters, pixel masks were automatically produced and used by the MEDFIT-IRAF tool for interpolation of the bad regions. We were forced to adopt this technique because of the noticeable worsening of the photometric accuracy we found in the experiments carried out with SExtractor when associated weight-mages were used to account for bad pixels and columns.

### 7.2. Background removal

To estimate the local background is a crucial step in order to achieve a good quality photometry. In our case the main problems related to the background removal reside in the presence of objects with extended halos (big early-type

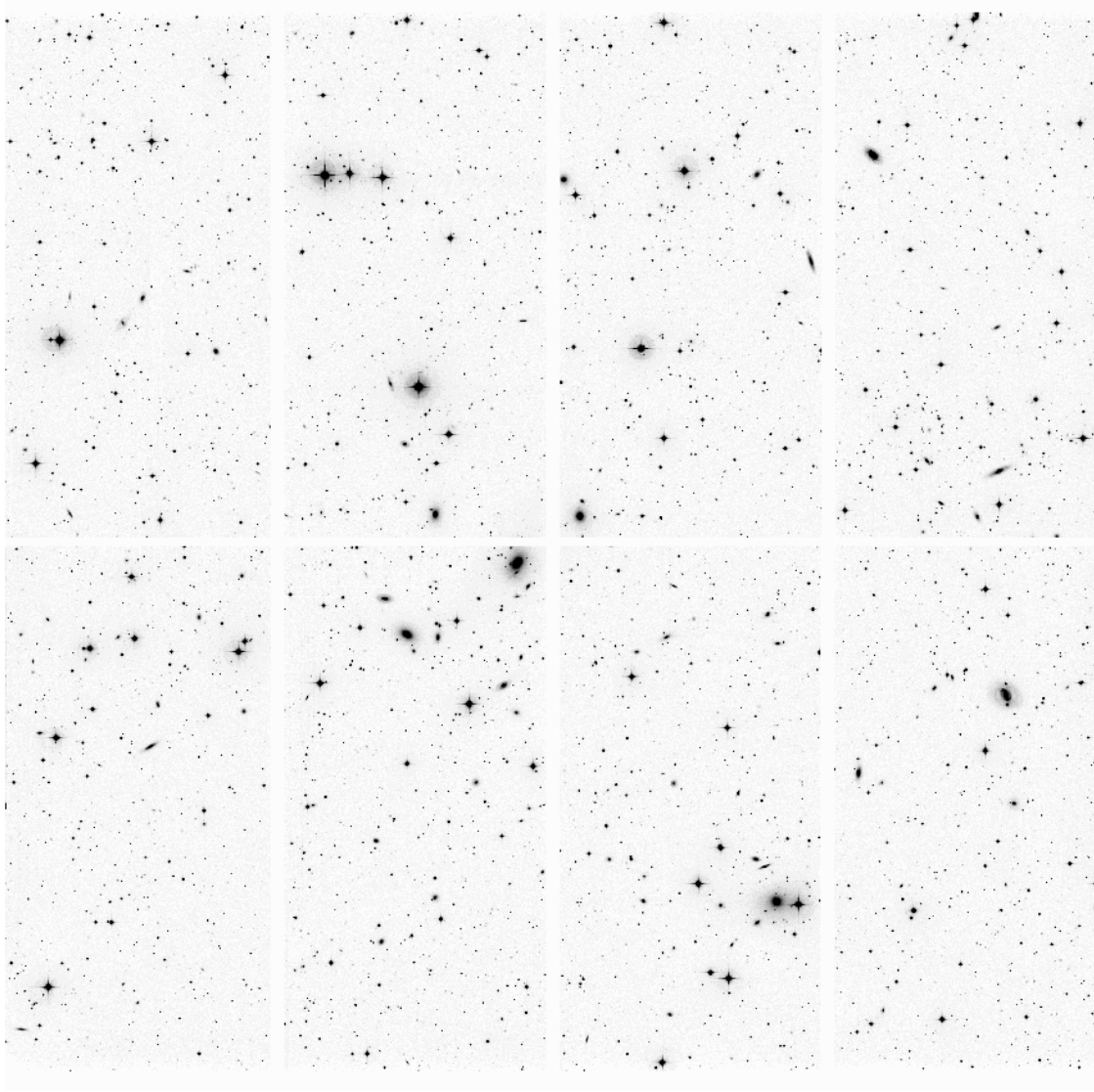


Fig. 9. Mosaic of the WFCM PG image of the cluster A 3556. North is up, East is left.

galaxies) or wings (very bright stars), as well as in the discontinuity of the background associated with the gaps between different CCDs of the mosaic. Both things are likely to produce artificial distortions of the background map to be removed from the mosaic, thus systematically biasing the local background estimates.

We exploited the capabilities of SExtractor, as well as the ELLIPSE-IRAF tool to devise a semi-automatic, iterative procedure for optimal sky subtraction over CCD mosaics, even in case of crowded galaxy cluster fields, possibly including big halo galaxies and/or very bright stars. This procedure generates two images. The first is the original mosaic, after model subtraction of the big halo galaxies and very bright stars. The second image contains only the previously removed big/bright galaxies, where the masked pixels (neighbours or gaps) are replaced by models. These two images are suitable for processing

by SExtractor, since each contains homogeneously sized objects, without critical blendings.

### 7.3. Catalogues

The final photometric catalogues of the WINGS-OPT survey are obtained, for each cluster, by running SExtractor over the two previously described images in both wavebands and by merging the four resulting catalogues into a single master-catalog containing all the sources detected in both filters over the field. The magnitudes in the final catalogues are color corrected following the procedure outlined in Sec. 7 (equations 6 and 7).

At this stage, we tried to detect as many sources as possible using very broad detection parameters of SExtractor. In particular, we used a minimum detection area of 5 pixels and detection thresholds of 1.5 and 1.1 times the  $bkg$  for WFCM INT and WFCM PG imaging,

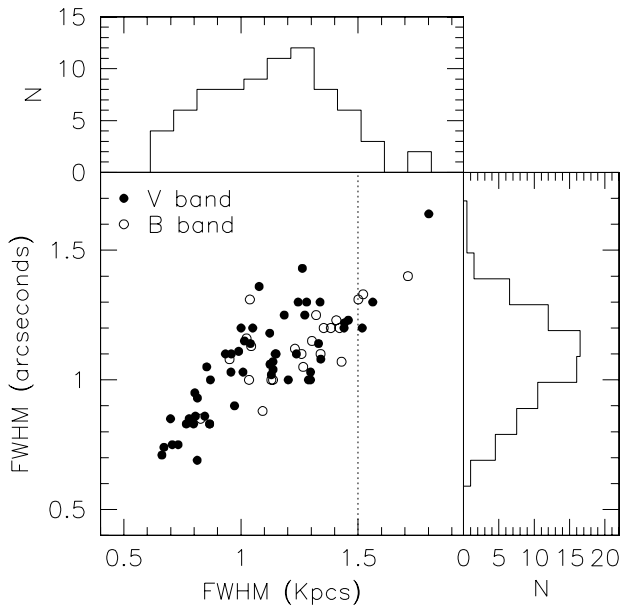


Fig. 10. Kpc vs. arcseconds FWHM and relative histograms for the W INGS-OPT imaging. Filled and open circles indicate that the best FWHM is achieved in the V and B band, respectively.

respectively, roughly corresponding to  $S/N = 4.5$  per square arcseconds in both cases.

In a forthcoming paper of the W INGS series we will present the W INGS-OPT catalogs, describing in detail the procedure we used to produce them, as well as the whole set of listed entries. Here we just mention that, on the basis of a few tags and of the automatic star/galaxy classifier (S/G) given by SExtractor, the master-catalog of each cluster has been preliminarily split into four catalogs: (i) a galaxy catalog (GCAT, S/G  $> 0.2$ ); (ii) a star catalog (SCAT, S/G  $> 0.8$ ); (iii) a catalog of objects with uncertain classification (UCAT,  $0.2 < S/G < 0.8$ ); (iv) a catalog of saturated stars (SSCAT). Afterwards, relying on multi-aperture photometry plotting tools and on visual inspection of the final images, the catalogs have been carefully cleaned, both removing the spurious detections (residual spikes and bad pixels, border effects, etc.) and moving misclassified objects from one catalog into another one (GCAT into SCAT and viceversa).

## 8. The W INGS-OPT data quality

In Sec. 4 the minimal requirements that the W INGS-OPT imaging survey should obey are mentioned, as far as both the spatial resolution (FWHM  $< 1.5$  Kpc) and the detection limit of absolute magnitude ( $M_V^{\lim} < 14$ ) are concerned. Using the photometric catalogues we can now check to what extent these requirements have been fulfilled by the actual W INGS-OPT data.

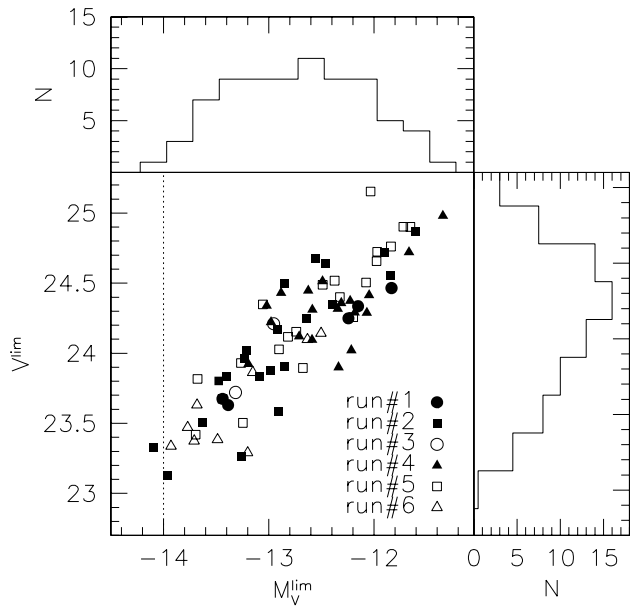


Fig. 11. Absolute vs. apparent V-band magnitudes at the detection limit and relative histograms for our W INGS-OPT observations. Different observing runs are plotted with different symbols, full and open symbols referring to WFC@INT and WFI@MPG observations, respectively.

## 8.1. Spatial resolution

In Figure 10 the spatial resolution, expressed as the FWHM in Kpc, is reported versus the FWHM in arcseconds for our W INGS-OPT observations. Apart from few very bad cases, the bulk of our cluster sample, in both arcseconds and Kpc, is located around FWHM  $\sim 1.1$  (see histograms in the figure). From Figure 10 it turns out that, in spite of the repeated observations taken in different runs, the spatial resolution of two clusters (A 1668, A 2626; 2% of the sample) largely exceeds the requirement described in Sec. 4.1. These clusters will be flagged out in the statistical analyses of surface photometry and morphology results.

## 8.2. Photometric depth

As far as the photometric depth of the survey is concerned, during the observing run # 2, fourteen clusters observed with good seeing, but in uncertain photometric conditions, were imaged again in good photometric conditions. The photometric, short exposures were used to calibrate the long exposures with uncertain photometry. For eight of these clusters the photometric adjustments turned out to be negligible in both filters, while for two clusters (A 970 and A 1069) a correction of 0.18 mag was needed in the B band only. Instead, the comparison with photometric exposures showed that strong adjustments (from 0.6 mag to 1.2 mag) in both bands were needed for the three clus-

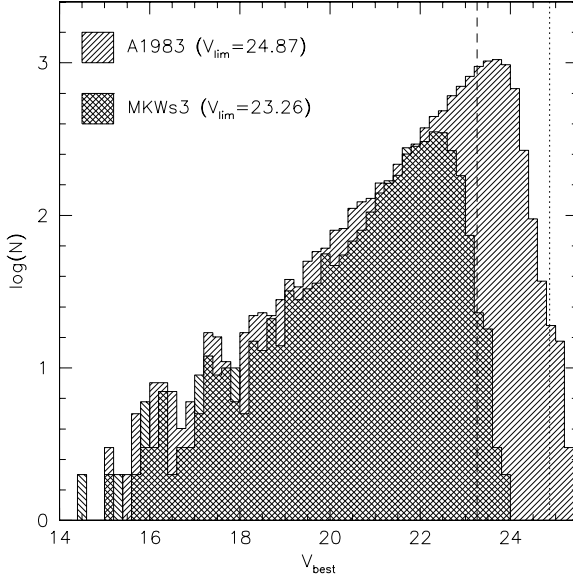


Fig. 12. V-band magnitude histograms of A1983 and MKW3s compared with the corresponding detection limit magnitudes computed using equation 8 (vertical lines).

ters A2149, A2271 and MKW3s, whose photometric depth turned out irreparably worsened.

In spite of that, it turns out from Figure 11 that the requested minimal absolute depth was practically achieved for all clusters in the WINGS-SOPT survey. Actually, the only case where  $M_V^{\text{lim}} < -14$  (A2149) exceeds the requested limit of just a few hundredths of magnitude. The detection limits reported in Figure 11 are computed using the formula:

$$m_{\text{lim}} = Z - 2.5 \log(\text{bkg} / \text{FWHM}_{\text{pix}}^2); \quad (8)$$

where  $Z$  is the photometric zero point,  $\text{bkg}$  is the rms of the background and  $\text{FWHM}_{\text{pix}}^2$  denotes how many  $\text{bkg}$  the detection is referred to (in Figure 11 we set  $= 1.5$  and  $= 1.1$  for WFC@INT and WFC@MPG observations, respectively). It is worth noticing that these 'theoretical' detection limits turn out to be in fair agreement with the corresponding histograms of apparent magnitudes obtained from the master-catalogs of clusters. This is well illustrated in Figure 12, where the V-band magnitude histograms for two clusters (A1983 and MKW3s) representing extreme cases of different photometric depth are compared with the detection limit magnitudes computed using equation 8. From Figure 12 it turns out that, even if there are detections well beyond the 'theoretical' limit, the completeness is achieved down to roughly half a magnitude brighter.

We also want to note that, according to what expected from the exposure time calculators, the average detection limits of WFC@INT and WFC@MPG observations turned out to be similar ( $< V_{\text{INT}}^{\text{lim}} > = 24.1$ ).

### 8.3. Internal photometric consistency

To check the internal consistency of the photometry given in the WINGS-SOPT master catalogs, determining at the same time how the photometric random errors depend on the flux, we compare in Figure 13 the magnitudes of stars in those clusters which have been observed in different nights of the same run, or in different runs with the same camera, or even with different cameras. Left, middle and right panels in Figure 13 show the magnitude differences as a function of the (average) magnitude itself for INT-INT, MPG-MPG and INT-MPG comparisons, respectively. Bottom panels of the same figure show the behaviour of the observed rms due to random errors as a function of the magnitude (dots), compared with the expected theoretical functions (dashed lines), computed using the proper, specific observational parameters.

The systematic magnitude shifts in Figure 13 are generally consistent with the expected zero point fluctuations among different observations (see Tab. 8). Also the random errors turn out to be in fair agreement with the expectations, apart from the INT-MPG comparison, where an additional source of scatter is present.

### 8.4. External photometric consistency

In order to perform an external consistency check of our photometric system, we have compared the magnitudes of stars in our master catalogs of Abell 119 (North) and Abell 2399 (South) with those provided for the same fields by the SDSS Sky Server. In the upper panels of Figure 14 the star magnitude differences  $V_{\text{WINGS}} - r_{\text{SDSS}}^0$  are reported as a function of the colors  $(B - V)_{\text{WINGS}}$  and these color-color plots are compared with the conversion equation (23) in Fukugita et al. (1996). In this figure just the stars brighter than  $V = 20$  are reported. The lower panels of Figure 14 reports, as a function of the magnitude, the differences between our  $V$  magnitudes and the corresponding SDSS ones, derived using the above mentioned equation.

The agreement between the two photometric systems turns out to be quite good and the random scatter as a function of the magnitude looks quite similar to that found in the case of the internal consistency check (see Figure 13).

### 8.5. Overall photometric quality

From Table 8 and from Figures 13 and 14 we conclude that the total (systematic plus random) photometric rms errors of our survey, derived by both internal and external comparisons are expected to vary from  $0.02$  mag, for bright objects, up to  $0.2$  mag, for objects close to the detection limit. However, it is worth noticing that, since the above analysis is based on magnitudes derived by SExtractor, it should be mainly referred to point sources. Actually, the systematic errors involved in the estimation of total galaxy magnitudes are known to depend on

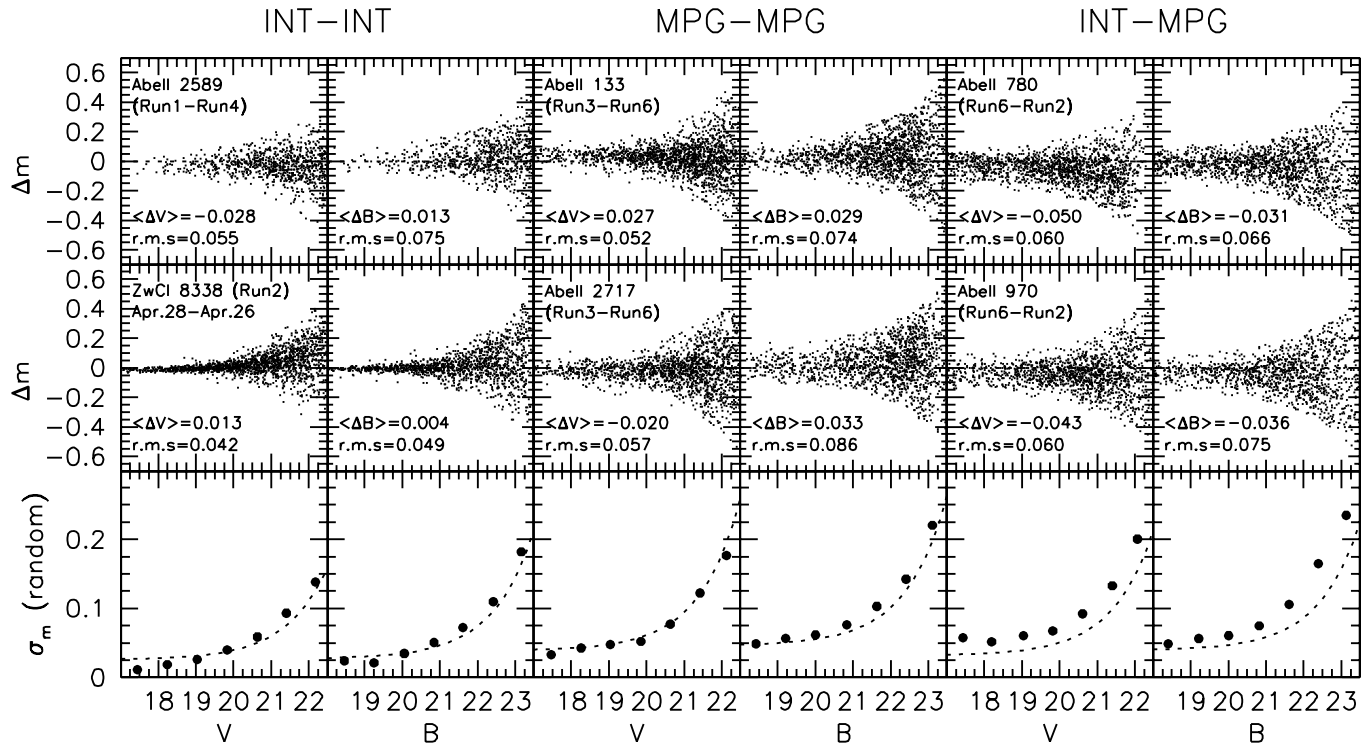


Fig. 13. Magnitude differences as a function of the (average) magnitude itself for INT-INT (leftmost two panels), MPG-MPG (central panels) and INT-MPG (rightmost two panels) comparisons in some clusters which have been observed in different nights of the same run, or in different runs with the same camera, or even with different camera. Bottom panels show the behaviour of the observed rms: due to random errors as a function of the magnitude (dots), compared with the expected theoretical functions (dashed lines), computed using the proper, specific observational parameters.

the galaxy light profile, as well as on the average surface brightness of galaxies (Franceschini et al. 1998). In a forthcoming paper of the series we will perform this analysis in the specific case of the WINGS-OPT survey. However, to illustrate the photometric quality of our galaxy data-set, even in the preliminary form provided by the WINGS-OPT master catalogs, we show in Figure 15 two examples of color-magnitude relations of WINGS clusters.

## 9. Summary and future plans

The WINGS-OPT observations we have presented here are part of an ambitious project aimed at providing the astronomical community with a huge database of galaxy properties in nearby clusters, to be used as a local benchmark for evolutionary studies.

We have described in detail our optical imaging, as well as the reduction procedures we used to manage the different issues typical of the wide-field mosaics. All the steps of the reduction sequence have been carefully checked for correspondence between expected and actual results and a special care has been paid to control the quality of astrometry and photometry. As far as the first issue is concerned, the typical rms of the astrometric errors is found

to be of the order of 0.2 arcseconds in both the northern and the southern observations. The photometric quality has been controlled using both internal and external consistency checks. In both cases the average differences among different observations turn out to be of the order of a few hundredths of magnitude, while the random photometric errors (rms) increase at increasing magnitude, from 0.02 mag for bright objects up to 0.2 mag for objects close to the detection limits. These are approximately found at 24 mag and 25 mag in the V and B bands, respectively, allowing us to sample the luminosity function of galaxies down to  $M_V = -14$  for almost all clusters and down to  $M_V = -13$  for roughly half sample.

We have also checked a posteriori whether the global quality of the WINGS-OPT imaging is actually fitting the minimum standards we proposed to ourselves a priori. We found that only for a few clusters the actual image quality (in terms of seeing and photometric depth) turns out to be marginally worse than the formal requirements.

The catalogs used to perform the above analyses have been produced for each cluster by running SExtractor onto the mosaiced frames in both filters. They contain position, shape and photometric parameters of several thousands of

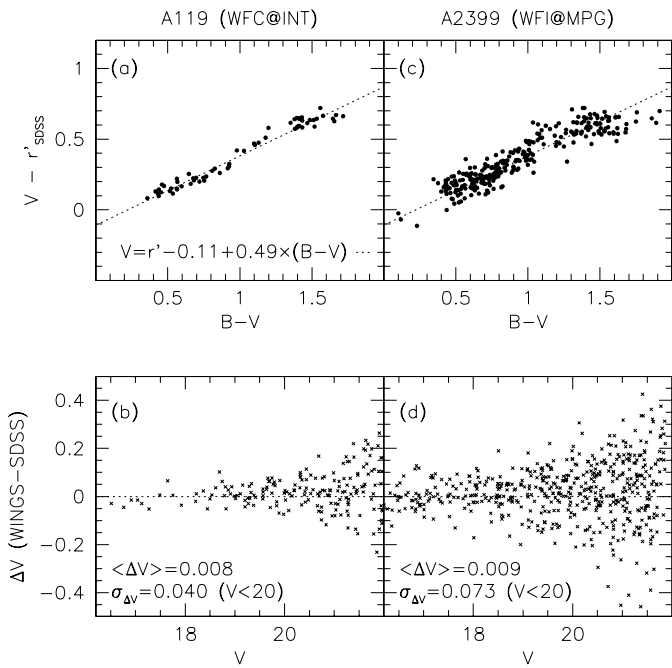


Fig. 14. Panels (a) and (c):  $V_{\text{WINGS}} - r'_{\text{SDSS}}$  as a function of  $(B - V)$  for the stars brighter than  $V = 20$  in the fields of Abell 119 (WFC@INT) and Abell 2399 (WFI@MPG). The dotted lines represent the color conversion proposed by Fukugita et al. (1996; eq. [23]). Panels (b) and (d): comparison between WINGS and SDSS magnitudes, after conversion of the  $r'$  (SDSS) magnitudes into the  $V$  band using the equation by Fukugita et al. (1996).

stars and galaxies in the cluster field. In this paper we have just outlined the complex procedure used to produce the catalogs. In a forthcoming paper we will go in more detail about catalogs, making them available for the whole astronomical community. Subsequent papers of the series will concern surface photometry and morphological classification of a subsample of large galaxies (more than 200 pixels above  $1.5 \text{ kpc}$ ), the global cluster properties (total luminosity and luminosity profile, characteristic radius, attorney) and the analysis of subclustering. Later, we will concentrate on the statistical properties of galaxies (luminosity function, color-magnitude,  $\log(R_e)$  and morphology-density relations) as a function of both the cluster properties and the environment (position inside the cluster and local density). In parallel, we plan also to produce the spectroscopic database, including redshifts and line indices of brightest galaxies, about 100 to 300 per cluster.

## References

Balogh, M. L., Morris, S. L., Yee, H. K. C., Carlberg, R. G., Ellingson, E., 1997, ApJ 488, L75

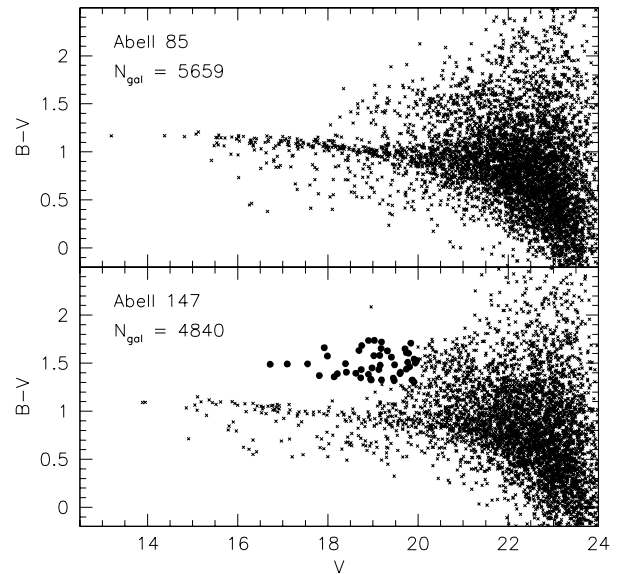


Fig. 15. Color-magnitude relations from the WINGS-OPTMASTER catalogs of the clusters Abell 85 and Abell 147. Note the second redder sequence in Abell 147 (full dots), which is likely to indicate the presence of a second galaxy cluster/group in the background

Balogh, M. L., Navarro, J. F., Morris, S. L., 2000, ApJ 540, 113  
 Balogh, M. L., Eke, V., Miller, C., Lewis, I., Bower, R., Couch, W., Nichol, R., Bland-Hawthorn, J., Baldry, I. K., Baugh, C., and 27 coauthors, 2004, MNRAS 348, 1355  
 Bertin, E., Arnouts, S., 1996, A & A 117, 393  
 Biviano, A., Katgert, P., Mazzarella, A., Males, M., den Hartog, R., Perea, J., Focardi, P., 1997, A & A 321, 84  
 Biviano, A., Mazzarella, A., Adamo, C., Katgert, P., den Hartog, R., de Theije, P., Rhee, G., 1999, A SPC 176, 15  
 Christlein, D., Zabludo, A. I., 2003, ApJ 591, 764  
 Couch, W. J., Ellis, R. S., Sharples, R. M., Smail, I., 1994, ApJ 430, 121  
 Couch, W. J., Barger, A. J., Smail, I., Ellis, R. S., Sharples, R. M., 1998, ApJ 497, 188  
 Couch, W. J., Balogh, M. L., Bower, R. G., Smail, I., Glazebrook, K., Taylor, M., 2001, ApJ 549, 820  
 De Propris, R., Colless, M., Driver, S. P., Couch, W., Peacock, J. A., Baldry, I. K., Baugh, C. M., Bland-Hawthorn, J., Bridges, T., Cannon, R., and 20 coauthors, 2003, MNRAS 342, 725  
 Desai, V., et al., 2005, in preparation  
 Dressler, A., 1980, ApJS 42, 565  
 Dressler, A., Oemler, A. Jr., Couch, W. J., Smail, I., Ellis, R. S., Barger, A., Butcher, H., Poggianti, B. M., Sharples, R. M., 1997, ApJ 490, 577  
 Dressler, A., Smail, I., Poggianti, B. M., Butcher, H., Couch, W. J., Ellis, R. S., Oemler, A. Jr., 1999, ApJS 122, 51

Ebeling, H., Voges, W., Böhringer, H., Edge, A. C., Huchra, J. P., Briel, U. G., 1996, MNRAS, 281, 799

Ebeling, H., Edge, A. C., Böhringer, H., Allen, S. W., Crawford, C. S., Fabian, A. C., Voges, W., Huchra, J. P., 1998, MNRAS, 301, 881

Ebeling, H., Edge, A. C., Allen, S. W., Crawford, C. S., Fabian, A. C., Huchra, J. P., 2000, MNRAS, 318, 333

Fasano, G., Poggianti, B. M., Couch, W. J., Bettoni, D., Kjørgaard, P., Møles, M., 2000, ApJ 542, 673

Fasano, G., Bettoni, D., D'Onofrio, M., Kjørgaard, P., Møles, M., 2002, A&A 387, 26

Fisher, D., Fabricant, D., Franx, M., van Dokkum, P., 1998, ApJ 498, 195

Franceschini, A., Silva, L., Fasano, G., Granato, G. L., Bressan, A., Amouts, S., Danese, L., 1998, ApJ 506, 600

Fukugita, M., Ichikawa, T., Gunn, J. E., Doi, M., Shimasaki, K., Schneider, D. P., 1996, AJ 111, 1748

Gomez, P. L., Nichol, R. C., Miller, C. J., Balogh, M. L., Goto, T., Zabludo, A. I., Romer, A. K., Bernardi, M., Sheth, R., Hopkins, A. M., and 7 coauthors, 2003, ApJ 584, 210

Hubble, E., Humason, M. L., 1931, ApJ 74, 43

Katgert, P., Mazure, A., Pereira, J., den Hartog, R., Møles, M., Le Fevre, O., Dubath, P., Focardi, P., Rhee, G., Jones, B., and 4 coauthors, 1996, A&A 310, 8

Katgert, P., Mazure, A., den Hartog, R., Adam, C., Biviano, A., Pereira, J., 1998, A&AS 129, 399

Kaumann, G., White, S. D. M., Heckman, T. M., Menard, B., Brinchmann, J., Charlot, S., Tremonti, C., Brinkmann, J., 2004, MNRAS 353, 713

Koch, A., Odenkirchen, M., Caldwell, J. A. R., G'rebel, E. K., 2003, ANS 324, 95

Landolt, A. J., 1992, AJ 104, 340

Lewis, I., Balogh, M., De Propris, R., Couch, W., Bower, R., O'Farrell, A., Bland-Hawthorn, J., Baldry, I. K., Baugh, C., Bridges, T., and 23 coauthors, 2002, MNRAS 334 673

Lubin, L. M., Postman, M., Oke, J. B., Ratnatunga, K. J., Gunn, J. E., Hoessel, J. G., Schneider, D. P., 1998, AJ 116, 584

Lubin, L. M., Oke, J. B., Postman, M., 2002, AJ 124, 1905

Mahdavi, A., Geller, M. J., 2001, ApJ 554, L129

Manfroid, J., Royer, P., Rauw, G., Gosset, E., 2001, A SPC 238, 373

Marmo, C., 2003, PhD Thesis, University of Padova

Marmo, C., Fasano, G., Pignatelli, E., Poggianti, B. M., Bettoni, D., Halliday, C., Varela, J., Møles, M., Kjørgaard, P., Couch, W., D'Onofrio, A., 2004, in Outskirts of Galaxy Clusters: intense life in the suburbs, IAU Coll. N. 195, ed. A. D. diaferio, p. 242

Mazure, A., Katgert, P., den Hartog, R., Biviano, A., Dubath, P., Escalera, E., Focardi, P., Gerbal, D., Giuricin, G., Jones, B., and 4 coauthors, 1996, A&A 310, 31

Møles, M., Garcia-Pelayo, J. M., Masegosa, J., Aparicio, A., Quintana, J. M., 1985, A&A 152, 271

Monet, D. G., 1998, Bulletin of the American Astronomical Society, Vol. 30, p. 1427

Muldchaey, J. S., D'Onofrio, M., Ushotzky, R. F., Burstein, D., 2003, ApJS 145, 39

Nichol, R. C., 2004, in Clusters of Galaxies: Probes of Cosmological Structure and Galaxy Evolution, from the Carnegie Observatories Centennial Symposium. Cambridge University Press, Edited by J. S. Mulchaey, A. D. Ressler, and A. Oemler, p. 24.

Oemler, A. Jr., 1974, ApJ 194, 1

Pignatelli, E., Fasano, G., Cassata, P., 2005, A&A, submitted

Pimbblet, K. A., Smith, I., Edge, A. C., Couch, W. J., O'Hely, E., Zabludo, A. I., 2001, MNRAS 327, 588

Poggianti, B. M., Smith, I., D'Onofrio, A., Couch, W. J., Barger, A. J., Butcher, H., Ellis, R. S., Oemler, A. Jr., 1999, ApJ 518, 576

Postman, M., Franx, M., Cross, N. J. G., Holden, B., Ford, H. C., Illingworth, G. D., Goto, T., Demarco, R., Rosati, P., Lakeslee, J. P., and 32 coauthors, 2005, ApJ 623, 721

Reiprich, T. H., Böhringer, H., 2002, ApJ, 567, 716

Simard, L., et al., 2005, private communication

Smith, I., D'Onofrio, A., Couch, W. J., Ellis, R. S., Oemler, A. Jr., Butcher, H., Sharples, R. M., 1997, ApJS 110, 213

Smith, R. M., Martnez, V. J., Graham, M. J., 2004, ApJ 617, 1017

Stetson, P. B., 2000, PASP 112, 925

Stone, R. C., Pier, J. R., Monet, D. G., 1999, AJ 118, 2488

Struble, M. F., Ftaclas, C., 1994, AJ 108, 1

Struble, M. F., Rood, H. J., 1991, ApJS 77, 363

Valdes, F. G., 1998, A SPC 145, 53

van Dokkum, P. G., Franx, M., Fabricant, D., Illingworth, G. D., Kelson, D. D., 2000, ApJ 541, 95

Varela, J., 2004, PhD Thesis, Complutense University of Madrid

Vogeley, M. S., Hoyle, F., Rojas, R. R., Goldberg, D. M., 2004, in Outskirts of Galaxy Clusters: Intense Life in the Suburbs. Edited by Antonaldo diaferio, IAU Colloquium 195, p. 5-11

Wu, X.-P., Fang, L.-Z., Xu, W., 1998, A&A, 338, 813